DETERMINATION OF THE ACOUSTIC PROPERTIES OF FROZEN SOILS

Y. Nakano, M. Smith,
R. Martin, H. Stevens
and
K. Knuth

May 1971

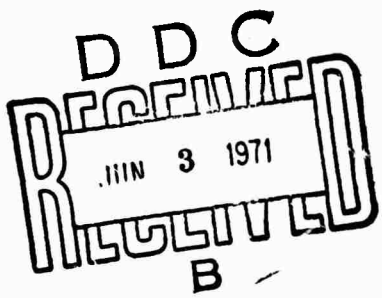

PREPARED FOR
ADVANCED RESEARCH PROJECTS AGENCY
ARPA ORDER 1525
BY

CORPS OF ENGINEERS, U.S. ARMY
COLD REGIONS RESEARCH AND ENGINEERING LABORATORY
HANOVER, NEW HAMPSHIRE

73

Unclassified
Security Classification

DOCUMENT CONTROL DATA - R & D

(Security classification of title, body of abstract and indexing annotation must be entered when the overall report is classified)

1. ORIGINATING ACTIVITY *(Corporate author)*
U.S. Army Cold Regions Research and Engineering Laboratory
Hanover, New Hampshire 03755

2a. REPORT SECURITY CLASSIFICATION
Unclassified

2b. GROUP

3. REPORT TITLE
DETERMINATION OF THE ACOUSTIC PROPERTIES OF FROZEN SOILS

4. DESCRIPTIVE NOTES *(Type of report and inclusive dates)*

5. AUTHOR(S) *(First name, middle initial, last name)*
Yoshisuke Nakano; Martin Smith, Jr.; Randolph Martin; Henry W. Stevens; Kurt V. Knuth

6. REPORT DATE	7a. TOTAL NO. OF PAGES	7b. NO. OF REFS
May 1971	70	49

8a. CONTRACT OR GRANT NO.	9a. ORIGINATOR'S REPORT NUMBER(S)
b. PROJECT NO.	
c. ARPA Order 1525	9b. OTHER REPORT NO(S) *(Any other numbers that may be assigned this report)*
d.	

10. DISTRIBUTION STATEMENT
Approved for public release; distribution unlimited.

11. SUPPLEMENTARY NOTES	12. SPONSORING MILITARY ACTIVITY
	Advanced Research Projects Agency

13. ABSTRACT

The acoustic properties of frozen earth materials were investigated. The study consists of four different efforts described in four sections. In the first part the velocities of dilatational waves were measured with the pulse first-arrival technique. In the second part a linear viscoelastic constitutive equation was obtained by the use of the resonance column technique. In the third part the method of free oscillation of spherical specimens was developed. In the last part the acoustic properties were determined by the use of a critical angle tank.

14. KEY WORDS

Acoustic properties
Complex modulus
Critical angle tank
Elastic waves
Free oscillation
Frozen soils
Viscoelasticity

DD FORM 1 NOV 68 1473 REPLACES DD FORM 1473, 1 JAN 64, WHICH IS OBSOLETE FOR ARMY USE.

Unclassified
Security Classification

CONTENTS

ILLUSTRATIONS

CONTENTS (Cont'd)

ILLUSTRATIONS (Cont'd)

TABLES

DETERMINATION OF THE ACOUSTIC PROPERTIES OF FROZEN SOILS

I. ULTRASONIC VELOCITIES OF DILATATIONAL WAVES IN FROZEN SOILS

by

K. Knuth, M. Smith, R. Martin and Y. Nakano

Introduction

Measuring the variation of the acoustic properties of solids under variable physical conditions has become well established as an effective method for investigating the physical structure of solids.

Although the acoustic properties of metals, plastics, and unfrozen earth materials have been widely explored, little attention has been directed toward frozen earth materials in the past. Recently there has been considerable interest in frozen earth because of military applications, such as seismic monitoring and personnel sensor detection in cold environments, and construction engineering applications, such as the Trans-Alaskan pipeline construction.

One of the most important acoustic properties of solids is the velocity of dilatational waves. A summary of dilatational wave velocity data obtained in permafrost regions was compiled by Barnes (1963). Eykov (1966) reviewed Russian works. Several laboratory studies on the subject have been reported (Frolov, 1961; Mullet, 1961; Kaplar, 1963; Desai and Moore, 1967; Timur, 1968). Frolov (1961) measured velocities of 30 kHz dilatational waves in four different types of frozen soils (sand, clay, sandstone and silt) in the temperature range from -20°C to 20°C. Muller (1961) measured the velocity in water-saturated sand and clay of various porosities as a function of decreasing temperature. His results indicate that with increasing ice content the velocity decreases for sand and increases for clay. Kaplar (1963) measured both dilatational and shear wave velocities in various frozen earth materials in the temperature range from 0°C to -20°C by the resonant bar method, in which either flexural, longitudinal or torsional vibrations were induced by electromagnetic means.

Recently Timur (1968) measured dilatational wave velocities in various earth materials between 26°C and -36°C by the pulse first-arrival technique, in which the time required for an elastic wave to traverse a sample of known length is determined. He measured velocities with both descending and ascending temperature and found that the two measurements generally do not agree, the degree of discrepancy depending on the specimen. It has recently been shown that freezing and thawing bring about a dramatic redistribution of water and a reorientation of particles, particularly in fine-grained earth media such as clay (Anderson and Hoekstra, 1965a and 1965b; Anderson and Tice, 1970). It is possible to consider a hysteresis of velocity reported by Timur (1968) as a result of such structural change in the specimen.

This report covers the first phase of an investigation of the relationship between acoustic properties of frozen soils and soil structure as well as constituents. The velocities of dilatational waves in three standard soils were measured with the pulse first-arrival technique. A hysteresis of velocities similar to that obtained by Timur was observed.

Experimental Procedure

Sample preparation

Three standard types of soils, 20-30 Ottawa sand, Hanover silt and Goodrich clay, were tested under fully water-saturated conditions. Figure 1 shows the gradation curves obtained according to ASTM (American Society for Testing and Materials) test procedures. We prepared circular cylindrical samples, either 2.5 cm diameter × about 15 cm length or 2.5 cm diameter × about 90 cm length. To prepare sand or silt, dry soil was first packed into 1-inch Tygon tubing encased in a copper jacket and was tamped or vibrated until a specified dry density was attained. Then water was sucked into the sample by the use of vacuum. To prepare clay, water-saturated clay was packed into Tygon tubing in order to maintain uniform density throughout the sample. After the ends of the tubing were sealed with aluminum plugs, the sample protected by the tubing and the copper jacket was frozen. When the sample was ready for testing, the copper jacket was removed and the plugs were replaced with transducer assemblies.

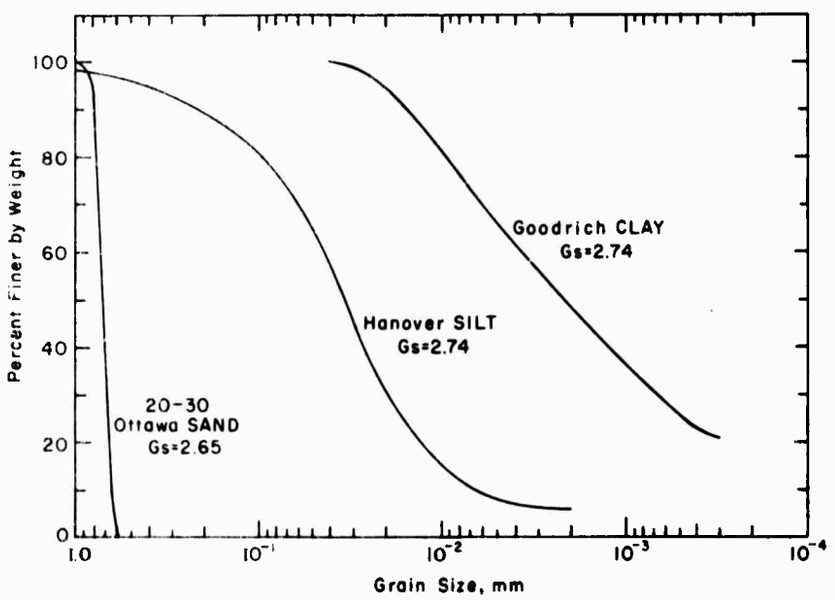

Figure 1. Gradation curves for 20-30 Ottawa sand, Hanover silt, and Goodrich clay. G_s = specific gravity.

Temperature control

Copper-constantan thermocouples were inserted to the center of the sample to monitor temperature. To maintain a constant temperature during the experiment, a Forma Scientific Model 2095 bath was used. The sample was placed in a cooling jacket, through which the cooling fluid was circulated by a pump via the bath. The temperature of the sample was kept constant within ±0.1 °C.

Velocity measurement

The velocities of propagating waves in the sample were measured with the pulse first-arrival technique (Kolsky, 1963). At either end of the sample a transducer of 0.5-inch-diameter ×

0.25-inch-thick PZT4, which was bonded to an aluminum disk 1 inch in diameter and 0.25 inch thick with silver epoxy, was attached to the surface of the sample with a few drops of silicone oil for better coupling. One of the transducers served as a transmitter and the other as a receiver.

A Hewlett Packard Model 214A pulse generator supplied pulses of about 1 second duration to the transmitter with a repetition rate of 500 to 1000 pulses per second. The receiver, which was connected to a Tektronix 50A dual-trace oscilloscope via a Krohn-Hite Model 3202 filter, displayed the received signal. A filter was used in a bandpass mode passing 10 kHz to 1 MHz. The other oscilloscope trace was used for a Computer Measurements Company Model A11 digital time delay generator providing accurate measurements of arrival time with an error of less than ±0.1 sec. Both traces on the oscilloscope were triggered by the pulse generator. This system was checked by the use of a standard medium, such as water, copper or aluminum, prior to measurements on frozen soils. All tests gave velocities within 1% of handbook values.

Accuracy of the pulse method

The behavior of elastic waves in any bounded medium necessarily entails various effects due to the presence of the boundaries. The effects of boundaries in circular cylinders have been well studied (Kolsky, 1963). Figure 2 depicts the theoretical group velocity of the first six axially symmetric modes in an aluminum rod 1.5 inches in diameter. The calculations were performed

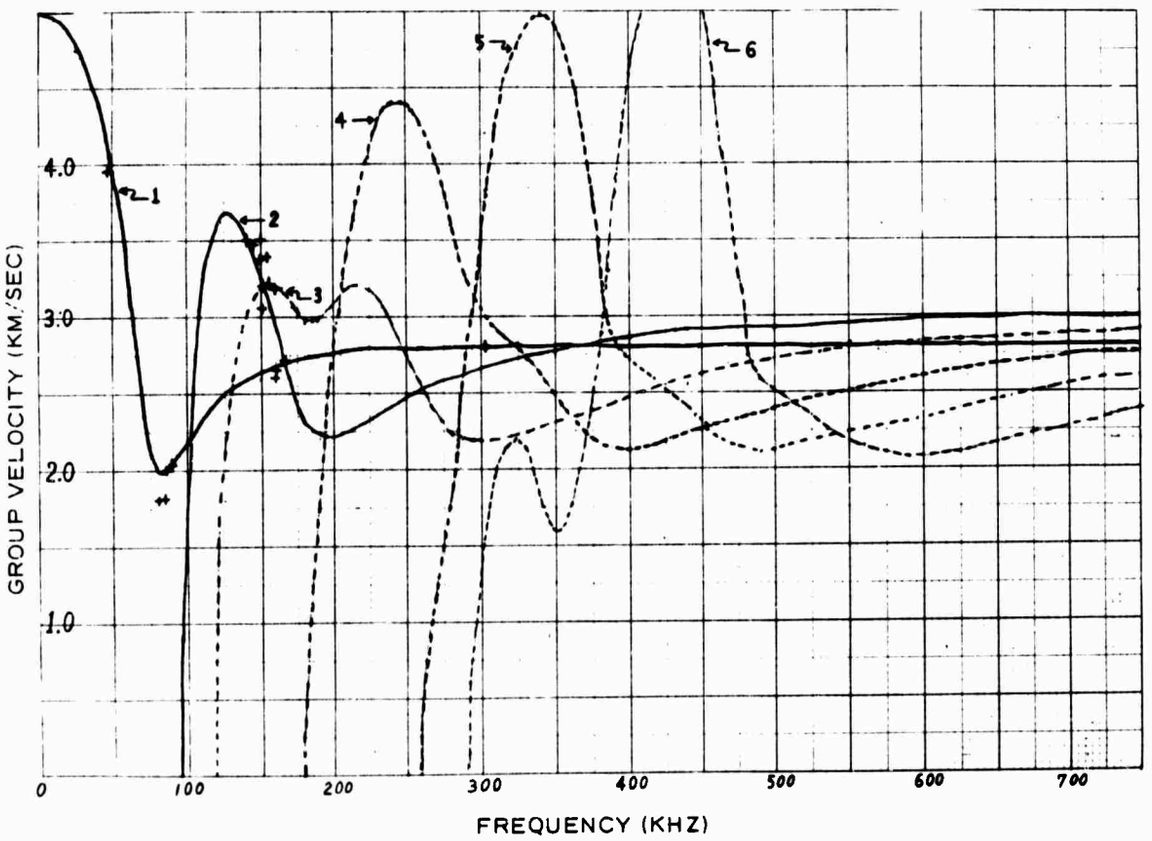

Figure 2. Group velocity versus frequency for a circular cylinder 1.5 in. in diameter, having a compressional velocity of 6.42 km/sec. The expected "bar" velocity is 3.04 km/sec. The crosses are observed group velocities in a 1.5 in. aluminum rod, 327.5 cm long.

using handbook values for shear and dilatational velocities. The lowest mode approached the bar velocity in the low-frequency limit. It is clear from Figure 2 that the mode structure of a cylinder is fairly complex. The crosses represent observations of group arrival versus frequency taken, with our apparatus, on a 327.5-cm aluminum rod, 1.5 inches in diameter. The primary uncertainty in the data lies in the assigned frequency, which was obtained by a period measurement of adjacent peaks. The agreement is quite satisfactory within the limits imposed by this error. The spurious points at about 80 kHz may be attributable to mode coupling at the rod's support points although we did not attempt to verify this.

As is seen in Figure 2, successively higher modes possess group velocity maxima which increase in both frequency and velocity. In a general way, these maxima approach the dilatational velocity of an elastic medium increasingly closely. For example, the 14th mode possesses a maximum at 1.15 MHz and a velocity of 97% of dilatational velocity.

In view of these calculations dilatational wave travel-time measurements should be made at the highest feasible frequency. Care should be taken to ensure operation in a region where the group velocity is close enough to the dilatational velocity to achieve the desired accuracy.

So far we have discussed the accuracy of the method applied for elastic solids. Since any real material deviates from an ideal elastic solid in one way or another, the accuracy of the method also depends on the anelastic behavior of the solids examined.

Results and Discussion

The results of the experiment are presented in Figures 3-5 where dilatational velocities are plotted as a function of temperature. Originally we intended to evolve a technique that would allow simultaneous measurement of both dilatational and shear velocities using long samples based

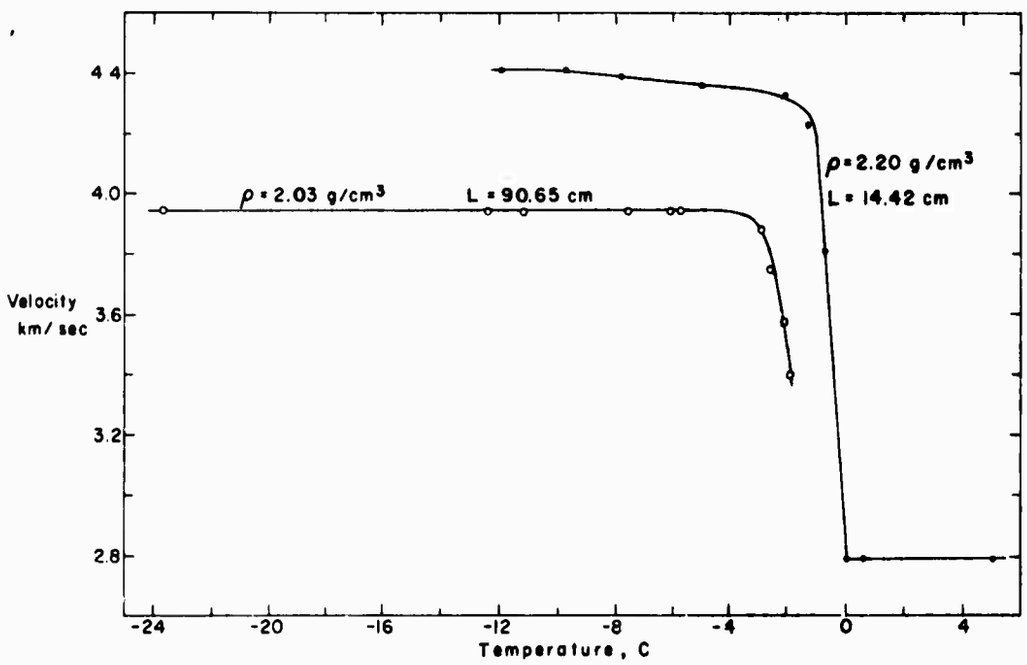

Figure 3. Dilatational velocity vs temperature for Ottawa sand. The differences in density and velocity reflect the difference in porosity.

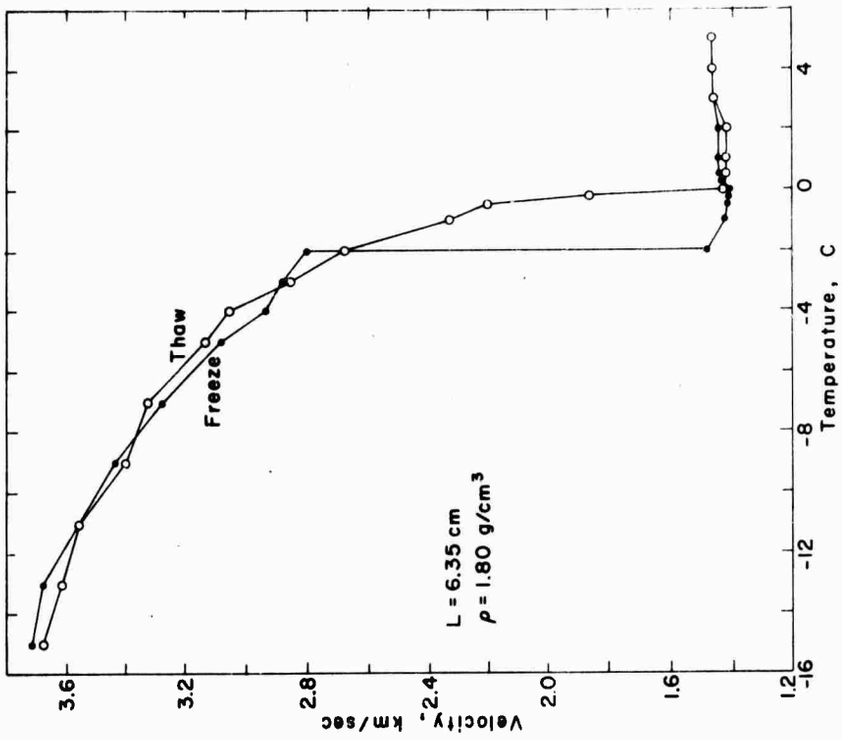

Figure 5. Dilatational velocity vs temperature for Goodrich clay.

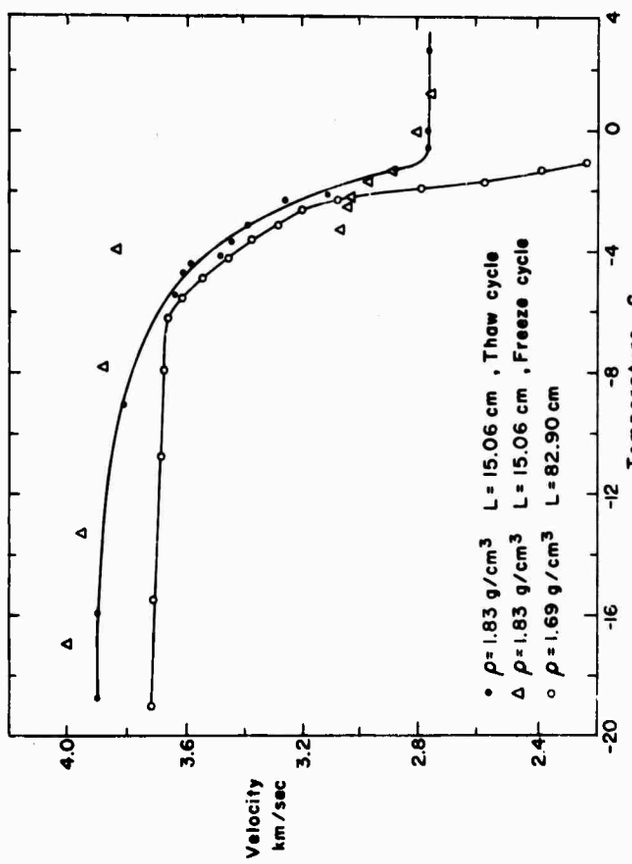

Figure 4. Dilatational velocity vs temperature for Hanover silt. The differences in density and velocity reflect the difference in porosity. Notice hysteresis in a thaw-freeze cycle.

upon the theory of guided elastic waves in a cylinder. This effort has been unsuccessful due to unexpected high attenuation in the samples tested. For Ottawa sand and Hanover silt, 90-cm-long samples barely allowed measurement of dilatational velocities in the frozen state, and did not allow measurement in the unfrozen state. Ninety-cm-long Goodrich clay did not yield any reliable measurement even in the frozen state. Despite the limited experimental data, we are able to present the following observations.

Velocity versus temperature curves

The decrease in dilatational wave velocity as an initially frozen water-saturated soil is thawed appears to be a direct consequence of the change in state of the water. Consider the soil as a two-component mixture, that is, a granular framework whose interstitial spaces are filled with water. A high-frequency wave traveling along any path through the sample will travel part of the time through the crystalline framework and part of the time through either water or ice, depending on the temperature. Since the dilatational wave velocity is about 3.0 km/sec in polycrystalline ice but only 1.49 km/sec in water, we expect that the travel time along the same path in a frozen sample will be less than the corresponding travel time in the thawed sample. The velocity of a wave propagating in the crystalline framework is essentially constant over this temperature range. Hence, the observed velocity for frozen soil should be greater than for the same sample thawed.

In light of this explanation of the variations of dilatational velocity in saturated soil as a function of temperature, it might be asked whether or not the observed change in velocity is in some way proportional to the amount of water in the sample. This suggests that perhaps each component contributes to the observed slowness in proportion to its relative abundance in the sample and the average compressional wave velocity of the individual components. Averaging techniques for two-component systems have been employed successfully to obtain compressibilities and moduli of many minerals which are available only in small quantities or in finely divided particles not suitable for bulk testing. They are first mixed with an isotropic material with known elastic constants. The unknown elastic parameter is then computed from the average properties of the composite material (Anderson, 1963; Chung and Buessman, 1967; Brace et al. 1969). The most notable method is to use Voigt and Reuss averages to obtain upper and lower bounds and then select a composition for which the spread of the bounds is a minimum. These methods however are not directly applicable in a straightforward way to the simple averaging of dilatational wave velocities for a two-component system.

Timur (1968) measured the dilatational wave velocity in water-saturated porous sandstone as a function of temperature. He observed a change in velocity similar to the one we observed as the temperature of the sample was increased from -24°C to +24°C. Moreover, only an insignificantly small decrease in velocity was observed on a dry sandstone sample as the temperature was raised from below the freezing point of water to room temperature. These observations also strongly suggest that the change in dilatational velocity as a frozen sample is thawed is attributable solely to the state of water in the pore spaces of the rock. Using an argument similar to the one we outlined above to explain the variation in velocity as our samples thawed, Timur (1968) proposed a simple time-averaging method to compute the theoretical velocity of a two-component system based on the percentage of each component in the sample and the velocity of that component. This technique assumes that the travel time for a dilatational wave through the sample is the travel time for each component computed according to

$$\frac{1}{v_0} = \frac{A}{v_1} + \frac{1 - A}{v_2} \qquad (1)$$

where v_0 is the observed velocity for the sample, v_1 and v_2 are the velocities of each component, and A is the relative volume of one component. For a water-saturated sample, the relative volume of water present is equal to the porosity of the sample.

Applying eq 1 to his results, Timur found good agreement with his experimental results. Typically the observed velocity fell within 5% of the predicted value. Our results on 20-30 Ottawa sand with a porosity of 37.5% (Fig. 3) were compared with the predicted velocities obtained using the time-averaging equation. For the frozen soil the predicted and observed values agreed to better than 2%. However, for saturated soil above 0°C agreement was poor. The observed velocity was 2.78 km/sec whereas the predicted value using time-averaging was not immediately applicable to the silt sample because the composition and relative abundance of the solid particles were not known.

The inapplicability of the time-averaging technique to unfrozen, saturated soil presents a difficulty. Why does the time-averaging method appear to be satisfactory for both frozen and unfrozen porous rocks but only to frozen Ottawa sand? The fact that the compressional wave velocity is less than the anticipated value based on time-averaging in thawed soil but in good agreement for frozen soil suggests that the compressional velocity is largely determined by the compressibility of the interstitial water rather than by the compressibility of the mineral solids. It appears then that for a consolidated and lithified elastic continuum, such as a porous rock, the solid and liquid can be time-averaged in direct proportion to their relative volumes to obtain a realistic value. In the case of a non-lithified, unfrozen soil, however, time averaging does not seem to apply due to the discontinuous nature of the mineral grains.

Hamilton (1970) studied the velocity of water-saturated marine sediments as a function of porosity and grain diameter. He found that the velocity typically increased from about 1.50 km/sec to 1.86 km/sec as the porosity was decreased from 80 to 30%. A similar increase in velocity was observed when the grain diameter was increased from 1 to 1000μ. Applying the time-averaging equation to Hamilton's results for sand produces no agreement between the predicted and observed results. Our results and those obtained by Hamilton suggest that time averaging is not an applicable method for predicting velocities in water-saturated soils. The breakdown of the time-averaging approach to velocities when the solid minerals do not form an interconnected framework suggests that further justification, on a sound physical basis, is required before time averaging can be accepted wholeheartedly even for frozen soils.

Ideally we would like to have a single theory that would predict the velocity in both frozen and unfrozen soils using easily measured properties of the components such as relative abundance, mineral composition, velocity of the minerals, and other readily obtainable elastic properties. Presently no such theory exists. As a major protion of our future research effort on the geophysical properties of frozen soils, this problem will be analyzed in detail both empirically and analytically to achieve a workable relation between porosity, mineral composition, water content and sample velocity.

Hysteresis in the velocity during a freeze-thaw cycle

It is evident that a strong correlation exists between dilatational velocities and unfrozen water content. Then it might be asked whether or not the observed hysteresis in the velocity during a freeze-thaw cycle is also caused by the hysteresis of unfrozen water content. The low-temperature phase composition of interfacial water has been a topic of continuing interest. Nersesova and Tsytovich (1963) conducted experimental investigations to determine the phase composition of water in various frozen soils by calorimetric methods. Unfrozen water contents obtained by them for typical non-saline soils are shown in Figure 6. In granular soil, pores are comparatively large and

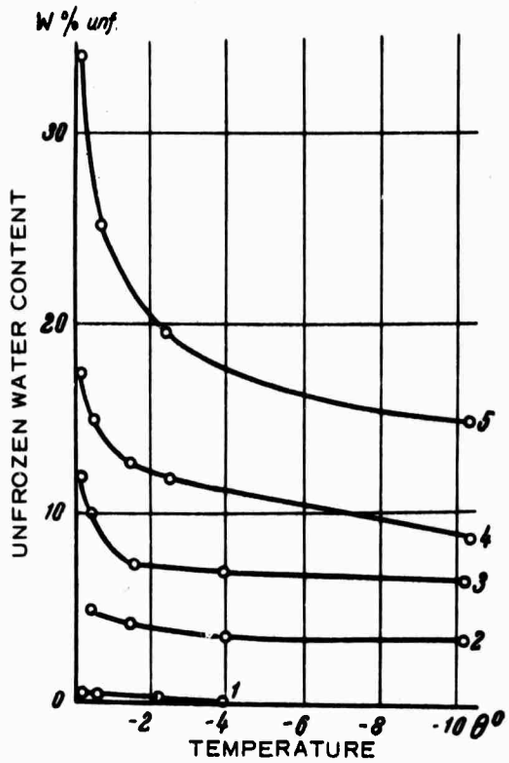

Figure 6. Unfrozen water contents in typical non-saline soils: 1) quartz sand, 2) sandy loam, 3) loam, 4) clay, and 5) clay containing montmorillonite.

almost all of the water freezes at the freezing point of water. However, clay and silt have fine pores, in which a significant portion of the water remains unfrozen in a liquid or semiliquid state. Those observations are consistent with the velocity-temperature relation.

Several studies concerning phase composition have been reported. However, the hysteresis of phase composition during a freeze-thaw cycle has not been discussed explicitly, because equilibrium phase composition has been the main subject. Anderson and Hoekstra (1965a, 1965b) have recently shown that freezing and thawing bring about a dramatic redistribution of water and a reorientation of particles in clay. They studied the changes in apparent d (001) spacing in Wyoming bentonite during the freeze-thaw cycle by X-ray diffraction. They found the hysteresis loop in the spacing during the freeze-thaw cycle due mainly to supercooling. However, if, during cooling, the sample was nucleated artificially the d (001) spacing dropped immediately and the cooling and warming curves nearly coincided. The d (001) spacing indicates the amount of interlamellar water constituting the gel structure. Freezing altered the gel structure and most of the interlamellar water was expelled on complete freezing; as a result, ice must form in extralamellar regions. If the interlamellar water corresponds to the "unfrozen" water (Anderson and Hoekstra, 1965a, 1965b), the hysteresis of unfrozen water can occur most probably in laboratory experiments, where no control on nucleation is made. Since almost no interlamellar water exists in granular sand, such as Ottawa sand, it is consistent that we did not observe any hysteresis in velocities for Ottawa sand.

Although the unfrozen water content is one of the most important variables in determining dilatational velocities in fine-grained frozen soils, determining the amount of unfrozen water is quite elaborate. Efforts have been initiated to evolve a technique allowing simultaneous determination of acoustic velocities and unfrozen water contents.

Literature Cited

Anderson, D.M. and P. Hoekstra (1965a) Migration of interlamellar water during freezing and thawing. *Soil Science Society of America Proceedings*, vol. 29, p. 498-504.

Anderson, D.M. and P. Hoekstra (1965b) Migration of interlamellar water during freezing and thawing of Wyoming bentonite. U.S. Army Cold Regions Research and Engineering Laboratory (USA CRREL) Research Report 192.

Anderson, D.M. and A.R. Tice (1970) Low-temperature phases of interfacial water in clay-water systems. USA CRREL Research Report 290.

Anderson, D.W. (1967) The interface ice and silicate surfaces. *Journal of Colloid and Interface Science*, vol. 25, no. 2.

Anderson, O. (1963) A simplified method for calculating the Debye temperature from elastic constants. *Journal of Physics and Chemistry of Solids*, vol. 24, p. 909-917.

Barnes, D.F. (1963) A review of geophysical method for delineating permafrost. *Proceedings of International Conference on Permafrost at Lafayette, Indiana*, 349N355.

Brace, W.F.; C.H. Scholz and P.N. LaMori (1969) Isothermal compressibility of byanite, andalusite and silimanite from synthetic aggregates. *Journal of Geophysical Research*, vol. 74, no. 8.

Desai, K.P. and E.J. Moore (1967) Well log interpretation in permafrost. *Transactions of the Professional Well Log Analysis.*

Frolov, A.D. (1961) Raspostnenie ul'trazubka v merzlykh oheschano glinistykh porodakh. Izv. An. SSSR Ser. Geof., no. 5.

Hamilton, E.L. (1970) Sound velocity and related properties of marine sediments. *Journal of Geophysical Research*, vol. 75, no. 23, p. 4423-4426.

Kaplar, C.W. (1963) Laboratory determination of dynamic moduli of frozen soils and of ice. *Proceedings of International Conference on Permafrost at Lafayette, Indiana*, p. 293-301.

Kolsky, H. (1963) *Stress waves in solids.* New York: Dover Pub., p. 213.

Muller, G. (1961) Geschwindigkeitsbestimmungen elastischer Wellen in gefrorenen Gesteinen und die Anwendung akustischer Messungen auf Untersuchungen des Frostmantels an Gefrierschachten. Geophys. Prosp., no. 9, p. 276-295.

Nersesova, Z.A. and N.A. Tsytovich (1963) Unfrozen water in frozen soils. *Proceedings of the Permafrost International Conference*, National Academy of Science, National Research Councel, Washington, D.C., p. 230.

Timur, A. (1968) Veolocity of compressional waves in porous media at permafrost temperatures. *Geophysics*, no. 33, p. 584-595.

Zykov, IV.D. (1966) Ultrasonic methods used in the study of elastic properties of frozen ground samples. Materialy VIII Vaseoiuz. Mezhduvedo mstvenuogo soveshchaniia po geokriologii, Yakutsk Vyp 5, p. 129-138.

II. DETERMINATION OF A LINEAR VISCOELASTIC CONSTITUTIVE EQUATION FOR FROZEN EARTH MATERIALS BY THE USE OF THE RESONANCE COLUMN TECHNIQUE

by

Y. Nakano and H. Stevens

Introduction

During the past decade considerable emphasis in soil mechanics research has been placed on the behavior of soils under dynamic loading. This behavior depends strongly on the nature of loading: stress, stress rate, frequency, etc. Consequently, various experimental techniques have been developed to determine the dynamic behavior of soils subjected to a specific kind of loading. Among these, the resonance column technique has been extensively used to investigate unfrozen soils under relatively weak harmonic loading (stress less than 100 psi) in the frequency range of 10^{-1} - 10^{4} Hz (Hardin and Richart, 1963; Hardin and Mossbarger, 1966; Hardin and Black, 1968; Hardin and Drnevich, 1970).

In the resonance column method a cylindrical column of material is subjected to a steady sinusoidal loading, either in the torsional or longitudinal mode. When a specimen of soil is under vibrational loading, the stress-strain relation creates a hysteresis loop. Two parameters have been used to define this relation (Hardin and Drnevich, 1970). These parameters are the modulus defined by the slope of a line through the ends of the loop, and the area of the loop, which is a measure of the damping capacity of the soil. Another way of defining the stress-strain relation is to determine the complex modulus according to linear viscoelastic theory (Lee, 1963; Hardin, 1965).

The dynamic behavior of frozen soils is less complex than that of unfrozen soils; but no comprehensive description of either material has been obtained. One useful and practical approach towards a quantitative description of dynamic behavior is determination of a constitutive relation based upon mechanics of continua. Stevens (1967) used a linear viscoelastic model for interpreting resonance column experiments and determined complex shear and Young's moduli. In his experiments the maximum dynamic stress in the specimen was varied from 0.1 psi to about 5.0 psi, where the complex modulus was found to be weakly dependent on the stress level. Despite such non-linear behavior in frozen soils, the linear viscoelastic constitutive equation is considered a good first approximation under low stress loading. In the present work, efforts were made to determine the simplest linear viscoelastic constitutive equation that can describe the dynamic behavior of frozen soils under both torsional and longitudinal vibrations consistently. In practical applications we encounter various types of disturbance: steady and unsteady disturbances, plane and surface waves, and cylindrical and spherical waves. Once the constitutive equation is determined, it is possible to predict the response of frozen soils subjected to such disturbances.

Experimental Determinations of Complex Modulus

In a linear viscoelastic material, when the stress σ varies sinusoidally with time at an angular frequency ω the strain ϵ varies with time at the same frequency but there is a phase lag δ between stress and strain. The stress and strain relation for linear viscoelastic solids is generally expressed by the following equation:

$$\sigma = E\epsilon \tag{1}$$

where E is defined as the complex Young's modulus and is a function of ω. The complex shear modulus G is defined similarly. We describe a method of determining these complex moduli in the following.

Method of test

A vertical cylinder of soil is subjected to steady-state sinusoidal vibration in the torsional or longitudinal mode at the lower base end with the other end free except for a light, relatively rigid cap. The input and output stress waves are observed and measured by piezoelectric accelerometers attached to the base plate and cap plate at each end of the specimen. The peak acceleration and the frequency are recorded. The drive frequency may be any value above the so-called "rigid body frequency" and within the limits of the drive motors, if the phase angle between input and output waves can be accurately measured; otherwise, the specimen must be excited at a known resonance. The ratio of output to input amplitudes and the frequency, together with the specimen properties of density and length, are required to compute the desired parameters.

Apparatus

The complete test apparatus includes a device for holding the specimen, drive motors and transducers for measuring the response, control and readout instrumentation, and auxiliary molds and equipment for specimen preparation. This apparatus has been discussed in detail by Hardin (1966) and Stevens (1967). At present the apparatus does not include a pressure cell, and the specimens are tested unconfined.

Computation of complex moduli and results

First we consider longitudinal vibration. If the wavelength of the standing wave is long in comparison with the diameter of the specimen, a rod condition is approximately true. The equation of motion for longitudinal vibration is:

$$E\frac{\partial^2 u}{\partial x^2} = \rho\frac{\partial^2 u}{\partial t^2} \tag{2}$$

where

E = complex Young's modulus

ρ = density of the medium

t = time

u = displacement along the coordinate x

x = coordinate (Lagrangian).

At the driven end $x = 0$ the system is given a sinusoidal displacement, namely,

$$u(0, t) = u_0 e^{i\omega t} \tag{3}$$

At the other end $x = L$ the effect of the mass of the cap resting on top of the specimen is considered:

$$SE \frac{\partial u(L, t)}{\partial x} = -m \frac{\partial^2 u(L, t)}{\partial t^2} \tag{4}$$

where

S = cross-sectional area of the specimen

m = end mass.

Solving eq 2 with the boundary conditions, eq 3 and 4, we obtain the following relationship for the ratio of bar end displacements (or accelerations), z:

$$z = \left|\frac{u(L, t)}{u(0, t)}\right| = \left|\frac{\sec pL}{1 - \gamma \tan pL}\right| \tag{5}$$

where

$$p^2 = \frac{\rho\omega^2}{E}$$

$$\gamma = \frac{m\omega^2}{pSE} .$$

In more detail (Norris and Young, 1970):

$$\mathrm{Re}(z^{-1}) = \cosh\left(\xi \tan\frac{\delta}{2}\right)(\cos\xi - Q_L \xi \sin\xi) + \\ + Q_L \xi \tan\frac{\delta}{2} \cos\xi \sin\left(\xi \tan\frac{\delta}{2}\right) \tag{6a}$$

$$\mathrm{Im}(z^{-1}) = \sinh\left(\xi \tan\frac{\delta}{2}\right)(\sin\xi + Q_L \xi \cos\xi) + \\ + Q_L \xi \tan\frac{\delta}{2} \sin\xi \cos\left(\xi \tan\frac{\delta}{2}\right) \tag{6b}$$

where

$$\delta = \frac{\mathrm{Im}(E)}{\mathrm{Re}(E)}$$

$$\xi = \frac{\omega L}{V_{lp}}$$

$$V_{lp} = \text{phase velocity} = \sqrt{\frac{E}{\rho}} \sec \frac{\delta}{2}$$

$$Q_L = \frac{m}{\rho S L}.$$

The condition of specimen resonance occurs when the ratio z is a maximum. As the frequency is increased from zero, the first maximum is the fundamental resonance and successive maximums indicate the harmonics. For the condition of resonance, where z is a maximum and z^{-2} is a minimum,

$$\frac{\partial}{\partial \xi}(z^{-2}) = 0. \tag{7}$$

Equations 5 and 7 may be solved simultaneously with a computer using an iterative process for the expressions and tan $(\delta/2)$. At each resonance point we can determine the complex Young's modulus from observed values of ω and z.

The equation for torsional vibration is perfectly analogous. In the torsional mode Q_L is replaced by Q_t, which is defined as

$$Q_t = \frac{r_c^4 \rho_c L_c}{r^4 \rho L} \tag{8}$$

where

r = radius of the specimen

r_c = radius of the cap

ρ_c = density of the cap

L_c = length of the cap.

The dynamic stress in the sample varies along its length as a damped sine wave, with the maximum at the node nearest the bottom or input end. At resonance, this node is very close to the bottom plane of the sample and the stress computed for correlative purposes is computed for the bottom plane.

It is difficult or impossible to accurately control the stress in the sample during the test because of the resonance phenomenon. Closest control can be obtained by keeping the input acceleration level g constant. As g is directly proportional to frequency and a wide frequency range is required, it is not very practical to control g at a relatively high value.

Consequently, no attempt is made to keep either stress or g constant. Instead, the drive force is held constant while the frequency is varied over its entire range. Then the drive force is increased an arbitrary amount, and so on. Thus we ensure measurements over a range of stress levels without knowing in advance what the values will be.

The frequencies at which measurements are taken cannot be predetermined, as only the resonant condition is used and resonant frequency varies with sample mass and stiffness. The first four or five resonances are usually used.

It is desirable to determine the moduli and loss angles for a given frequency and a given stress or strain, not only because these relationships are required, but to allow comparisons between values

for different samples. To accomplish this, modulus and tan δ are each plotted versus the computed dynamic stress at one resonance. A smooth curve is drawn through the points and the modulus of tan δ value picked off for a given stress. The resonance frequency is obtained by interpolating between the two adjacent measured frequencies. If, say, four resonances are used, four values at four frequencies at a constant stress are obtained. A plot of modulus or tan δ versus frequency is then prepared and a smooth curve drawn through these points. A value for modulus or tan δ for a given frequency and a given stress can then be obtained. The same process is used to obtain values for about three stress levels and at least three frequencies.

Usually, the test measurements plot in such a way that there is little question as to the shape of the curve drawn through the points. However, scatter does occur, particularly for the tan δ measurements. Some guidelines are used in drawing the curves. It is assumed that the modulus decreases or is constant with increasing stress and increases or is constant with increasing frequency. Tan δ is assumed to increase with increasing stress but there are no good guidelines for the relationship to frequency. Usually, the trend is to a decrease with increasing frequency but at times there is a strong trend to a maximum peak at a particular frequency within the test range. The results of the experiment are presented in Table I. The specimens tested included several standard frozen soils as well as polycrystalline ice. The following variables are also listed in the table:

L = length of specimen (cm)

D = diameter of specimen (cm)

ρ_w = wet (total) density (g/cm^3)

W = water content (g water/g dry soil) (%)

ρ_D = dry density (g/cm^3)

P_0 = porosity (void volume/total volume) (%)

V_d = void ratio (void volume/dry soil volume) (-)

S_w = saturation (water) (%)

S_i = saturation (ice) (%)

T = test temperature (°C)

f = frequency (kHz)

E^* = absolute value of complex Young's modulus (Kbar)

V_{lp} = phase velocity of longitudinal wave (km/sec)

G^* = absolute value of complex shear modulus (Kbar)

V_{tp} = phase velocity of torsional wave (km/sec)

σ_D = dynamic stress imposed on the bottom circumference of the specimen (psi).

The values of E^* and G^* in the table are either interpolated or extrapolated from those at resonance frequencies in order to show the properties of different frozen soils at the same frequencies. The phase velocities, V_{lp} and V_{tp}, are computed based upon complex moduli E and G respectively. Gradation curves of the soils obtained using ASTM (American Society for Testing and Materials) test procedures are also presented in Figure 7.

Despite the limited data it is possible to describe some general trends in the dynamic behavior of frozen soils. Stevens (1967) found several important parameters affecting such behavior: soil type, ice content, void ratio and frequency.

Table I.

L = 49.45 Pb = 41.9
D = 7.538 Vd = 0.719
ρ_w = 1.946 Sw = 86.7
W = 22.9 Si = 96.1
ρ_s = 1.580 T = −3.89

3N1053 FROZEN MANCHESTER SILT

f	E*	$V_{\ell\rho}$	Tan δ_ℓ	G*	$V_{t\rho}$	Tan δ_t
			σ_p = 0.1			
1.00	158	2.85	0.0230	67.2	1.86	0.067
2.00	167	2.93	0.0227	68.3	1.88	0.056
5.00	175	3.00	0.0215	70.3	1.90	0.045
10.0	177	3.02	0.0167	70.9	1.91	0.045
			σ_p = 1.0			
1.00	158	2.85	0.0230	67.0	1.86	0.067
2.00	166	2.92	0.0227	68.3	1.87	0.056
5.00	175	3.00	0.0215	70.3	1.90	0.045
10.0	177	3.02	0.0167	70.7	1.91	0.045
			σ_p = 5.0			
1.00	146	2.74	0.0230	62.9	1.80	0.067
2.00	164	2.90	0.0227	68.0	1.87	0.056
5.00	175	3.00	0.0215	69.7	1.89	0.045
10.0	177	3.01	0.0167	70.3	1.90	0.045

L = 50.8 Pb = 34.0
D = 7.55 Vd = 0.516
ρ_w = 2.054 Sw = 90.2
W = 17.5 Si = 100.2
ρ_s = 1.749 T = − 3.89

3N1052 FROZEN 20-30 OTTAWA SAND

f	E*	$V_{\ell\rho}$	Tan δ_ℓ	G*	$V_{t\rho}$	Tan δ_t
			σ_p = 0.1			
1.00	319	3.94	0.023	137	2.59	0.049
2.00	333	4.03	0.021	138	2.59	0.047
5.00	356	4.17	0.019	139	2.60	0.037
10.0	358	4.18	0.014	139	2.61	0.032
			σ_p = 1.0			
1.00	319	3.94	0.023	136	2.57	0.051
2.00	333	4.03	0.021	137	2.58	0.048
5.00	356	4.17	0.019	137	2.59	0.041
10.0	358	4.18	0.014	139	2.60	0.037
			σ_p = 5.0			
1.00	319	3.94	0.027	135	2.57	0.097
2.00	333	4.03	0.025	136	2.58	0.088
5.00	356	4.17	0.021	137	2.58	0.063
10.0	358	4.18	0.014	138	2.59	0.041

Table I (Cont'd).

L = 40.6 P_b = 68.1
D = 7.44 V_d = 2.130
ρ_w = 1.433 S_w = 83.6
W = 66.0 S_i = 91.2
3N1028 FROZEN FAIRBANKS SILT UNDISTURBED ρ_s = 0.8619 T = −9.44

f	E*	V_{tp}	Tan δ_t	G*	V_{tp}	Tan δ_t
			σ_3= 0.1			
0.50	121	2.90	0.024	42.6	1.72	0.072
1.00	121	2.91	0.030	42.9	1.73	0.067
2.00	122	2.92	0.038	43.4	1.74	0.056
5.00	124	2.94	0.066	44.4	1.76	0.041
			σ_3= 1.0			
0.50	121	2.90	0.028	42.5	1.72	0.075
1.00	121	2.91	0.032	42.8	1.73	0.069
2.00	122	2.91	0.039	43.4	1.74	0.058
5.00	123	2.94	0.070	44.3	1.76	0.041
			σ_3= 5.0			
0.50	121	2.90	0.060	42.4	1.72	0.086
1.00	121	2.90	0.062	42.6	1.73	0.076
2.00	121	2.91	0.070	43.1	1.74	0.064
5.00	121	2.91	0.099	44.1	1.75	0.042

L = 50.6 P_b = 80.2
D = 7.44 V_d = 4.030
ρ_w = 1.235 S_w = 86.8
W = 130 S_i = 94.7
3N1027 FROZEN FAIRBANKS SILT UNDISTURBED ρ_s = 0.5367 T = −9.44

f	E*	V_{tp}	Tan δ_t	G*	V_{tp}	Tan δ_t
			σ_3= 0.1			
0.50	97.3	2.81	0.018	35.3	1.69	0.064
1.00	97.6	2.81	0.023	35.6	1.70	0.059
2.00	98.3	2.82	0.033	36.0	1.71	0.049
5.00	100	2.84	0.051	36.4	1.72	0.044
			σ_3= 1.0			
0.50	97.0	2.80	0.027	35.3	1.69	0.064
1.00	97.4	2.81	0.032	35.6	1.70	0.059
2.00	98.2	2.82	0.041	36.0	1.71	0.049
5.00	99.8	2.84	0.052	36.3	1.72	0.044
			σ_3= 5.0			
0.50	96.9	2.80	0.108	35.0	1.68	0.064
1.00	97.3	2.81	0.100	35.3	1.69	0.061
2.00	98.0	2.82	0.083	35.8	1.70	0.055
5.00	99.4	2.84	0.060	36.4	1.72	0.054

Table I (Cont'd).

L = 42.1 Pb = 60.7
D = 7.41 Vd = 1.545
ρ_w = 1.552 Sw = 80.3
W = 46.0 Si = 87.6
ρ_o = 1.062 T = -9.44

SN1026 FROZEN FAIRBANKS SILT UNDISTURBED

f	E*	V_{lp}	Tan δ_l	G*	V_{tp}	Tan δ_t
			σ_p = 0.1			
0.50	135	2.95	0.021	49.3	1.78	0.062
1.00	135	2.95	0.023	49.6	1.79	0.060
2.00	135	2.95	0.028	50.0	1.80	0.055
5.00	135	2.95	0.043	50.2	1.80	0.043
			σ_p = 1.0			
0.50	135	2.95	0.036	49.3	1.78	0.069
1.00	135	2.95	0.037	49.6	1.79	0.066
2.00	135	2.95	0.040	50.0	1.80	0.059
5.00	135	2.95	0.044	50.2	1.80	0.043
			σ_p = 5.0			
0.50	131	2.91	0.132	49.3	1.78	0.097
1.00	132	2.92	0.122	49.5	1.79	0.090
2.00	133	2.93	0.092	49.8	1.79	0.073
5.00	134	2.94	0.045	49.9	1.79	0.043

L = 40.0 Pb =
D = Vd =
ρ_w = 0.9072 Sw =
W = Si =
ρ_o = T = -9.44

SN1024 POLYCRYSTALLINE ICE MADE BY FREEZING WATER WITH SNOW

f	E*	V_{lp}	Tan δ_l	G*	V_{tp}	Tan δ_t
			σ_p = 0.1			
0.50	61.7	2.61	0.060	21.2	1.53	0.056
1.00	63.4	2.64	0.056	21.7	1.55	0.056
2.00	65.5	2.69	0.052	22.4	1.57	0.056
5.00	67.0	2.76	0.052	23.1	1.60	0.056
			σ_p = 1.0			
0.50	59.3	2.56	0.089	20.3	1.50	0.095
1.00	61.4	2.60	0.084	20.7	1.51	0.085
2.00	63.8	2.68	0.078	21.7	1.55	0.073
5.00	67.6	2.73	0.072	22.9	1.59	0.066
			σ_p = 5.0			
0.50	56.5	2.51	0.270	18.7	1.45	0.340
1.00	58.6	2.55	0.254	19.4	1.47	0.270
2.00	61.4	2.61	0.220	20.6	1.51	0.155
5.00	66.2	2.70	0.146	22.2	1.57	0.077

Table I (Cont'd).

SN1023 POLYCRYSTALLINE ICE MADE BY RAPID CRYSTALLIZATION OF WATER

L = 34.8 P_o =
D = V_d =
ρ_w = 0.9098 S_w =
W = S_i =
ρ_o = T = -9.44

f	E*	V_{lp}	Tan δ_l	G*	V_{tp}	Tan δ_t
			σ_o = 0.1			
1.00	88.8	3.12	0.055	29.0	1.78	0.017
2.00	88.8	3.12	0.041	29.2	1.79	0.015
5.00	88.8	3.12	0.020	29.3	1.80	0.013
			σ_o = 1.0			
1.00	88.3	3.12	0.079	28.5	1.77	0.037
2.00	88.3	3.11	0.062	28.9	1.78	0.026
5.00	88.3	3.11	0.027	29.3	1.79	0.014
			σ_o = 5.0			
1.00	87.9	3.13	0.333	27.9	1.75	0.065
2.00	87.9	3.12	0.397	28.4	1.77	0.045
5.00	87.9	3.11	0.131	29.2	1.79	0.017

SN1019 FROZEN-100 LEBANON TILL

L = 39.10 P_o = 36.2
D = 9.90 V_d = 0.568
ρ_w = 2.156 S_w = 91.8
W = 18.2 S_i = 101.6
ρ_o = 1.825 T = -9.44

f	E*	V_{lp}	Tan δ_l	G*	V_{tp}	Tan δ_t
			σ_o = 0.1			
0.50	228	3.26	0.105	89.3	2.04	0.040
1.00	229	3.27	0.086	89.3	2.04	0.038
2.00	232	3.28	0.062	89.3	2.04	0.033
5.00	240	3.34	0.032	94.5	2.10	0.018
			σ_o = 1.0			
0.50	222	3.22	0.146	88.6	2.03	0.086
1.00	223	3.23	0.126	88.6	2.03	0.077
2.00	226	3.24	0.093	88.6	2.03	0.060
5.00	234	3.30	0.040	93.8	2.09	0.022
			σ_o = 5.0			
0.50	216	3.20	0.370	87.9	2.03	0.317
1.00	218	3.20	0.340	87.9	2.03	0.277
2.00	221	3.22	0.272	87.9	2.03	0.188
5.00	225	3.24	0.080	91.7	2.07	0.024

Table I (Cont'd).

L = 38.22 P_b = 40.0
D = 9.888 V_d = 0.666
ρ_w = 1.753 S_w = 40.6
W = 10.2 S_i = 45.1
ρ_o = 1.591 T = -9.44

JJC17 FROZEN, 100-200, OTTAWA SAND

f	E*	V_{tp}	Tan δ_l	G*	V_{tp}	Tan δ_t
			σ_o = 0.1			
0.50	96.5	2.35	0.024	48.6	1.67	0.024
1.00	101	2.40	0.024	49.6	1.68	0.023
2.00	110	2.50	0.025	51.7	1.72	0.023
5.00	126	2.68	0.040	56.4	1.79	0.022
			σ_o = 1.0			
0.50	95.5	2.33	0.060	48.3	1.66	0.062
1.00	99.3	2.38	0.060	49.4	1.68	0.053
2.00	108	2.49	0.060	51.4	1.71	0.041
5.00	125	2.68	0.060	56.1	1.79	0.028
			σ_o = 5.0			
0.50	90.3	2.30	0.454	48.1	1.66	0.200
1.00	95.2	2.35	0.400	49.1	1.68	0.166
2.00	106	2.47	0.300	51.0	1.71	0.109
5.00	124	2.66	0.188	55.6	1.78	0.053

L = 38.19 P_b = 39.2
D = 9.903 V_d = 0.645
ρ_w = 1.966 S_w = 90.4
W = 22.0 S_i = 98.7
ρ_o = 1.612 T = -9.44

SN1014 FROZEN, 100-200, OTTAWA SAND

f	E*	V_{tp}	Tan δ_l	G*	V_{tp}	Tan δ_t
			σ_o = 0.1			
0.50	263	3.71	0.029	105	2.31	0.032
1.00	263	3.66	0.029	105	2.31	0.030
2.00	263	3.66	0.029	105	2.31	0.028
5.00	263	3.66	0.029	105	2.31	0.024
			σ_o = 1.0			
0.50	263	3.66	0.074	105	2.31	0.135
1.00	263	3.66	0.074	105	2.31	0.120
2.00	263	3.66	0.074	105	2.31	0.094
5.00	263	3.66	0.074	105	2.31	0.024
			σ_o = 5.0			
0.50	263	3.67	0.220	105	2.35	0.585
1.00	263	3.67	0.220	105	2.34	0.520
2.00	263	3.67	0.220	105	2.33	0.370
5.00	263	3.67	0.220	105	2.31	0.030

Table I (Cont'd).

L = 37.50 Pb = 46.9
D = 10.00 Vd = 0.885
ρ_w = 1.863 Sw = 92.9
W = 30.6 Si = 101.5
SN1012 FROZEN SUFFIELD CLAY ρ_s = 1.427 T = -9.44

f	E*	V_{ip}	Tan δ_l	G*	V_{tp}	Tan δ_t
			σ_0= 0.1			
0.50	75.2	2.01	0.088	25.8	1.18	0.072
1.00	75.9	2.02	0.090	26.9	1.20	0.076
2.00	82.3	2.10	0.104	27.8	1.22	0.090
5.00	81.7	2.10	0.146	29.8	1.27	0.170
			σ_0= 1.0			
0.50	75.2	2.01	0.120	25.8	1.18	0.105
1.00	75.9	2.02	0.121	26.9	1.20	0.105
2.00	82.3	2.10	0.123	27.8	1.22	0.106
5.00	81.7	2.10	0.146	29.8	1.27	0.170
			σ_0= 5.0			
0.50	75.2	2.02	0.275	25.8	1.18	0.157
1.00	75.9	2.03	0.250	26.9	1.20	0.160
2.00	82.3	2.11	0.202	27.8	1.22	0.175
5.00	81.7	2.10	0.124	29.8	1.27	0.195

L = 37.63 Pb = 50.0
D = 9.880 Vd = 0.962
ρ_w = 1.629 Sw = 51.6
W = 18.6 Si = 56.8
SN1007 FROZEN SUFFIELD CLAY ρ_s = 1.370 T = -9.44

f	E*	V_{ip}	Tan δ_l	G*	V_{tp}	Tan δ_t
			σ_0= 0.1			
0.50	14.8	0.952	0.087	5.86	0.600	0.124
1.00	18.8	1.07	0.105	7.10	0.661	0.130
2.00	22.0	1.16	0.140	7.45	0.680	0.305
			σ_0= 1.0			
0.50	13.0	0.893	0.140	5.86	0.600	0.140
1.00	17.6	1.04	0.148	7.10	0.661	0.148
2.00	21.8	1.16	0.150	7.45	0.680	0.150
			σ_0= 5.0			
0.50	10.8	0.821	0.360	5.24	0.571	0.320
1.00	15.9	0.996	0.360	6.83	0.651	0.320
2.00	20.5	1.13	0.365	7.31	0.675	0.370

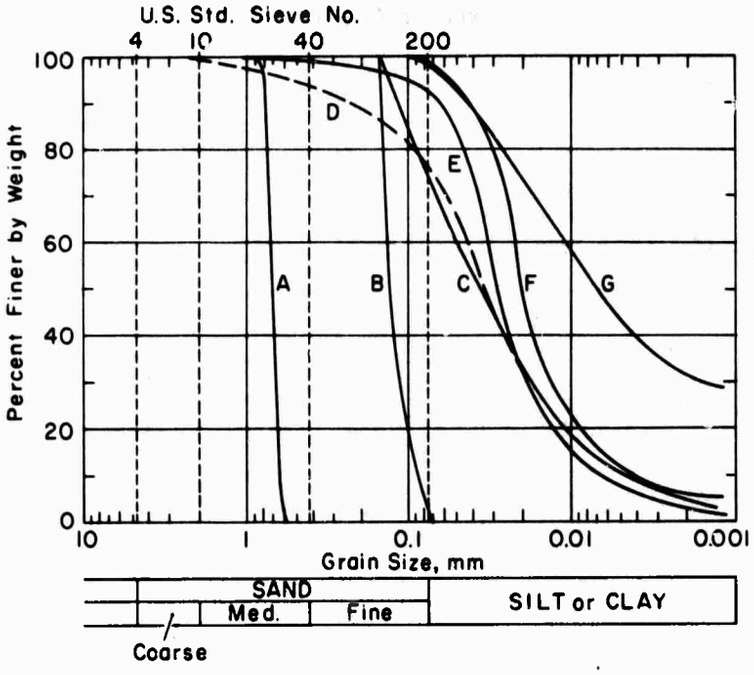

Curve	Description	Specific gravity	Liquid limit	Plastic limit	Plastic index	Non-plastic
A	20-30 Ottawa sand	2.65				X
B	--100-200 Ottawa sand	2.65				X
C	--100 Lebanon till	2.86				X
D	Hanover silt	2.74				X
E	Fairbanks silt	2.70				X
F	Manchester silt	2.73				X
G	Suffield clay	2.69	45.0	24.0	21.0	

Figure 7. Gradation curves.

For ice-saturated or almost saturated non-plastic frozen soils a strong correlation was found between modulus and void ratio (Fig. 8, 9). Since such frozen soils have only two constituents, soil minerals and ice, the moduli are bounded below by those of ice and above by those of rock. The moduli of several standard rocks measured by Simmons and Brace (1965) are plotted in these figures to show the upper bound.

Frozen soil specimens have a fundamental resonance of the order of 2.0 kHz longitudinally and 1.0 kHz torsionally. In this experiment soil was usually tested up to the third and fourth resonance. Therefore, the range of frequency is about 1.0 kHz to 10 kHz. In this range the modulus increases and tan δ decreases with increasing frequency. Tan δ is approximately a reciprocal of the quality factor Q, which is defined as the ratio of the energy carried by a wave to the energy dissipated per radius of phase shift (Thurston, 1964) and is commonly used by seismologists (Jackson and Anderson, 1970). For ice-saturated frozen soils the correlation between Q and void ratio is not so strong as that between modulus and void ratio.

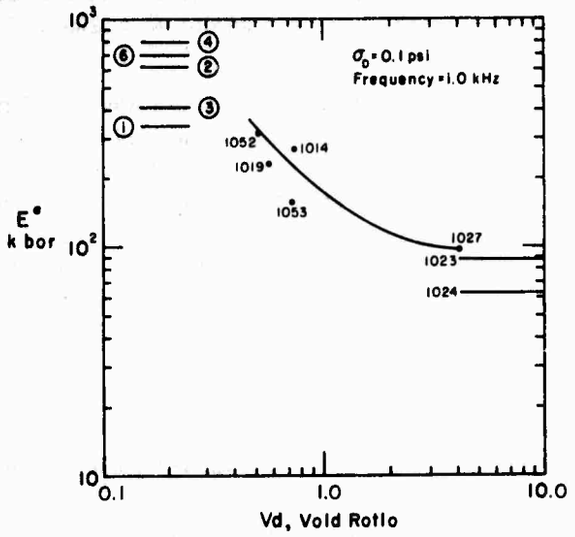

Figure 8. E vs void ratio. 1 Granite, Stone Mountain, Georgia. 2 Quartzite, Rutland, Vermont. 3 Granite, Westerly, Rhode Island. 4 Limestone, Oak Hall Quarry, Pennsylvania. 6 Fused quartz.*

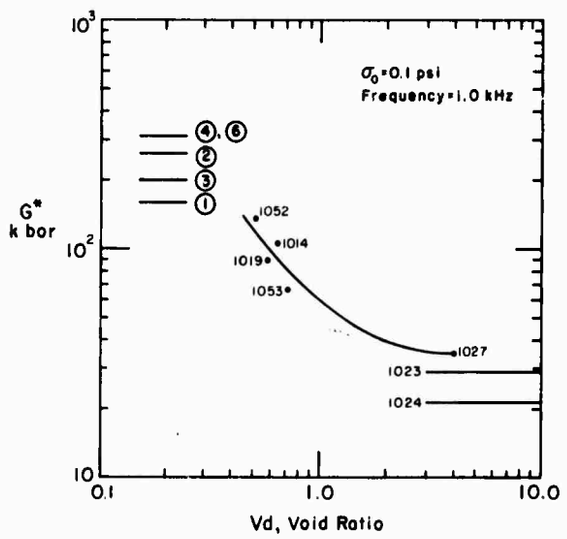

Figure 9. G vs void ratio. 1 Granite, Stone Mountain, Georgia. 2 Quartzite, Rutland, Vermont. 3 Granite, Westerly, Rhode Island. 4 Limestone, Oak Hall Quarry, Pennsylvania. 6 Fused quartz.*

Q values for frozen soils were found in the range of 10-100. They are bounded below by polycrystalline ice and above by solid rock, such as quartzite ($Q \simeq 250$) and granite ($Q \simeq 70$) (Volarovich and Gurvitch, 1957).

Although many theories concerning the attenuation of stress waves in earth materials have been proposed, none of them is definitive. The attenuation mechanism is difficult to pin down even in the laboratory, where measurements can be made as a function of frequency, temperature, pressure, purity, grain size, annealing history, etc. In the present work we used *viscosity* to describe anelastic properties of frozen soils. When applied to solids, this term usually means that stress relief and deformation occur by some poorly understood process, which may be a combination of several types of processes, and may result in linear or nonlinear internal friction of complicated (or unknown) frequency dependence (Jackson and Anderson, 1970). Further efforts are required to obtain complete understanding of attenuation in frozen soils.

Determination of Linear Viscoelastic Constitutive Equations from Measured Complex Modulus

The general constitutive equations of a linear viscoelastic solid are given as (Eringen, 1967)

$$R\sigma_{rr}\delta_{kl} + S\sigma_{kl} = P\epsilon_{rr}\delta_{kl} + 2Q\epsilon_{kl} \tag{9}$$

where σ_{ij}, ϵ_{ij} are stress and strain tensors respectively, and P, Q, R and S are linear operators defined as,

$$P = \lambda_0 + \sum_{i=1}^{N_1} \lambda_i \frac{\partial^i}{\partial t^i} \tag{10a}$$

$$Q = \mu_0 + \sum_{i=1}^{N_2} \mu_i \frac{\partial^i}{\partial t^i} \tag{10b}$$

$$R = \alpha_0 + \sum_{i=1}^{N_3} \alpha_i \frac{\partial^i}{\partial t^i} \tag{10c}$$

$$S = \beta_0 + \sum_{i=1}^{N_4} \beta_i \frac{\partial^i}{\partial t^i} \tag{10d}$$

where λ_i, μ_i, α_i and β_i are constants.

Torsional mode

Theory. We deal only with circular cylindrical specimens and use cylindrical coordinates for convenience. Let the coordinates be r, θ and z, with z being the axis of the cylindrical specimen, and let the corresponding displacements be u_r, u_θ and u_z. In the propagation of torsional waves, no longitudinal or lateral displacement is to be expected and the motion is symmetric about the axis of the cylinder. Therefore, u_r and u_z must both vanish and we need to consider only the wave equation for u_θ. If the torsional stress applied to the specimen varies sinusoidally with time and the strain thus induced also varies sinusoidally but with a phase difference, then we may write the wave equation for viscoelastic materials as:

$$\rho \frac{\partial^2 u_\theta}{\partial t^2} = G \frac{\partial^2 u_\theta}{\partial z^2} \tag{11}$$

where G is a complex shear modulus, ρ is the density of the specimen, and t is time.

The wave equation is also written in terms of the present linear viscoelastic model as:

$$\rho \frac{\partial^2 u_\theta}{\partial t^2} = \frac{\partial \sigma_{\theta z}}{\partial z} \tag{12a}$$

$$S\sigma_{\theta z} = Q \frac{\partial u_\theta}{\partial z} . \tag{12b}$$

Among many alternatives we selected the following four-parameter model for torsional vibration:

$$Q = \mu_1 \frac{\partial}{\partial t} + \mu_2 \frac{\partial^2}{\partial t^2} \tag{13a}$$

$$S = \beta_0 + \frac{\partial}{\partial t} + \beta_2 \frac{\partial^2}{\partial t^2} . \tag{13b}$$

If u_θ and $\sigma_{\theta z}$ are harmonic with an angular frequency ω, then the complex shear modulus G is given as

$$G = G_1 + iG_2 \tag{14}$$

where

$$G_1 = \frac{\omega^2[\mu_1 - \mu_2(\beta_0 - \beta_2\omega^2)]}{G_3} \tag{15a}$$

$$G_2 = \frac{\omega[\mu_1(\beta_0 - \beta_2\omega^2) + \mu_2\omega^2]}{G_3} \tag{15b}$$

$$G_3 = (\beta_0 - \beta_2\omega^2)^2 + \omega^2 . \tag{15c}$$

The phase velocity V_{tp} and the group velocity V_{tg} are obtained as follows:

$$V_{tp} = \sqrt{\frac{G^*}{\rho}} \sec\left(\frac{\delta_t}{2}\right) \tag{16a}$$

$$V_{tg} = \frac{\sqrt{\frac{G^*}{\rho}}}{\left[\cos\frac{\delta_t}{2} - \frac{1}{2}\omega\left(\frac{G^*_\omega}{G^*}\right)\cos\frac{\delta_t}{2} - \frac{1}{2}\omega\delta_{t\omega}\sin\frac{\delta_t}{2}\right]} \tag{16b}$$

where

$$G^* = |G| \tag{17a}$$

$$G^*_\omega = \frac{\partial G^*}{\partial \omega} \tag{17b}$$

$$\delta_t = \tan^{-1}\left(\frac{G_2}{G_1}\right) \tag{17c}$$

$$\delta_{t\omega} = \frac{\partial \delta_t}{\partial \omega}. \tag{17d}$$

The values of constants μ_1, μ_2, β_0 and β_2 are determined from the four observed variables, namely the complex modulus and the loss factor $L_s (= \tan \delta_t)$, at any two distinct frequencies. Since it is not generally expected that the model satisfies these four conditions exactly, the following scheme is used. Suppose the observed modulus and the loss factor at two distinct frequencies are $G^{(1)}$, $G^{(2)}$, $L_s^{(1)}$, and $L_s^{(2)}$ respectively; then find μ_1 and μ_2 which minimize the derivation V_t, defined as:

$$V_t = \frac{[(G^{(1)} - G_m^{(1)})^2 + (G^{(2)} - G_m^{(2)})^2]}{(G^{(1)2} + G^{(2)2})} \tag{18}$$

under the constraints

$$L_{sm}^{(1)} = L_s^{(1)} \tag{19a}$$

$$L_{sm}^{(2)} = L_s^{(2)} \tag{19b}$$

where G_m and L_{sm} are the complex modulus and the loss factor predicted by the model.

Results and discussion. The four parameters μ_1, μ_2, β_0 and β_2 were computed as follows. We used the observed modulus and the loss factors at 1.00 kHz and 2.00 kHz to compare the constitutive equations of different frozen soils around 1.5 kHz frequency. Since eq 19a and 19b are linear in terms of β_0 and β_2, we solved these equations to substitute μ_1 and μ_2 for β_0 and β_2 in eq 18. Now V_t is a function of μ_1 and μ_2 only; that is,

$$V_t = V_t(\mu_1, \mu_2). \tag{20}$$

When V_t is a minimum, we have

$$F(\mu_1, \mu_2) = \frac{\partial V_t}{\partial \mu_1} = 0 \tag{21a}$$

$$G(\mu_1, \mu_2) = \frac{\partial V_t}{\partial \mu_2} = 0. \tag{21b}$$

Suppose that $(\mu_1^{(1)}, \mu_2^{(1)})$ is an approximate solution and let $\delta\mu_1^{(1)}$ and $\delta\mu_2^{(1)}$ be corrections which we shall determine. Expanding F and G in a Taylor series and truncating after the first-order, we get:

$$F(\mu_1^{(1)}, \mu_2^{(1)}) + \delta\mu_1^{(1)} \frac{\partial F(\mu_1^{(1)}, \mu_2^{(1)})}{\partial \mu_1} + \delta\mu_2^{(1)} \frac{\partial F(\mu_1^{(1)}, \mu_2^{(1)})}{\partial \mu_2} = 0 \tag{22a}$$

$$G(\mu_1^{(1)}, \mu_2^{(1)}) + \delta\mu_1^{(1)} \frac{\partial G(\mu_1^{(1)}, \mu_2^{(1)})}{\partial \mu_1} + \delta\mu_2^{(1)} \frac{\partial G(\mu_1^{(1)}, \mu_2^{(1)})}{\partial \mu_2} = 0. \tag{22b}$$

This linear system in $\delta\mu_1^{(1)}$ and $\delta\mu_2^{(1)}$ gives the next approximation, $\mu_1^{(2)}$ and $\mu_2^{(2)}$, as

$$\mu_1^{(2)} = \mu_1^{(1)} + \delta\mu_1^{(1)} \tag{23a}$$

$$\mu_2^{(2)} = \mu_2^{(1)} + \delta\mu_2^{(1)}. \tag{23b}$$

The above iterative procedure is repeated until we obtain μ_1 and μ_2, which minimize V_t. The results of the computation are shown in Table II.

CGS units were used in the computation. For instance, stress was expressed in dynes/cm^2. The computation was quite satisfactory. An absolute minimum value of V_t exists for all specimens computed and convergence is rapid. In order to indicate the degree of approximation or error we listed $V_t^{1/2}$ in the table. The values of $V_t^{1/2}$ vary in the range of 10^{-2} to 10^{-3}, which is considered satisfactory. In the general constitutive relation, eq 9, if all other constants except λ_1, μ_1 and β_1 are vanishing and β_1 is equal to unity as defined, eq 9 reduces to the elastic constitutive equation, or Hooke's law in terms of an incremental strain resulting in an incremental stress, where λ_1 and μ_1 are Lamé constants. Therefore, μ_2, β_0 and β_2 indicate a degree of deviation from elastic solid. For ice-saturated or almost saturated non-plastic frozen soils a strong correlation was found between modulus and void ratio as described before. We plotted four parameters, μ_1, μ_2, β_0 and β_2, versus void ratio in order to find out some general trends (Fig. 10). It appears that a correlation exists between either μ_1 or μ_2 and void ratio, but neither β_0 nor β_2 are affected by variations of void ratio.

Longitudinal mode

Theory. If the wavelength of the harmonic wave is long in comparison with the diameter of the specimen, the equation of motion for longitudinal vibration in Cartesian coordinates is written as:

$$E \frac{\partial^2 u_x}{\partial x^2} = \rho \frac{\partial^2 u_x}{\partial t^2} \tag{24}$$

where

E = complex Young's modulus

ρ = density of the medium

t = time

u_x = displacement along x coordinate.

Table II. Values of constants for torsional mode.

(1) SN 1053 Manchester Silt

	0.5	1.0	5.0
λ_0			
μ_0	6.78×10^{10}	6.77×10^{10}	6.55×10^{10}
μ_1	4.76×10^{4}	4.76×10^{4}	4.68×10^{4}
β_1	3.27×10^{2}	3.27×10^{2}	3.27×10^{2}
β_2	-1.68×10^{-6}	-1.69×10^{-6}	-1.67×10^{-6}
$V_t^{1/2}$	8.22×10^{-3}	8.72×10^{-3}	3.85×10^{-2}

(2) SN 1052 Ottawa Sand

	0.1	1.0	5.0
λ_0			
μ_0	1.38×10^{11}	1.36×10^{11}	1.36×10^{11}
μ_1	1.45×10^{5}	1.45×10^{5}	1.91×10^{5}
β_1	2.14×10^{2}	2.26×10^{2}	4.44×10^{2}
β_2	-1.33×10^{-6}	-1.33×10^{-6}	-2.78×10^{-6}
$V_t^{1/2}$	1.31×10^{-3}	2.30×10^{-3}	1.79×10^{-3}

(3) SN 1028 Fairbanks Silt

	0.1	1.0	5.0
λ_0			
μ_0	4.32×10^{10}	4.31×10^{10}	4.30×10^{10}
μ_1	4.00×10^{4}	4.06×10^{4}	4.25×10^{4}
β_1	3.24×10^{2}	3.37×10^{2}	3.81×10^{2}
β_2	-1.43×10^{-6}	-1.50×10^{-6}	-1.69×10^{-6}
$V_t^{1/2}$	5.78×10^{-3}	5.10×10^{-3}	5.36×10^{-3}

(4) SN 1027 Fairbanks Silt

	0.1	1.0	5.0
λ_0			
μ_0	3.58×10^{10}	3.58×10^{10}	3.56×10^{10}
μ_1	3.41×10^{4}	3.41×10^{4}	3.81×10^{4}
β_1	2.89×10^{2}	2.89×10^{2}	2.81×10^{2}
β_2	-1.12×10^{-6}	-1.12×10^{-6}	-1.53×10^{-6}
$V_t^{1/2}$	4.61×10^{-3}	4.61×10^{-3}	6.33×10^{-3}

(5) SN 1026 Fairbanks Silt

	0.1	1.0	5.0
λ_0			
μ_0	4.98×10^{10}	4.99×10^{10}	4.98×10^{10}
μ_1	4.55×10^{4}	4.64×10^{4}	4.81×10^{4}
β_1	2.72×10^{2}	3.06×10^{2}	4.48×10^{2}
β_2	-1.74×10^{-6}	-1.83×10^{-6}	-2.00×10^{-6}
$V_t^{1/2}$	4.08×10^{-3}	4.00×10^{-3}	1.92×10^{-3}

(6) SN 1024 Polycrystalline Ice

	0.1	1.0	5.0
λ_0			
μ_0	2.21×10^{10}	2.12×10^{10}	2.04×10^{10}
μ_1	3.20×10^{4}	3.28×10^{4}	3.05×10^{4}
β_1	2.34×10^{2}	4.06×10^{2}	1.61×10^{3}
β_2	-1.52×10^{-6}	-1.69×10^{-6}	-6.22×10^{-7}
$V_t^{1/2}$	1.53×10^{-2}	2.18×10^{-2}	1.92×10^{-2}

(7) SN 1023 Polycrystalline Ice

	0.1	1.0	5.0
λ_0			
μ_0	2.91×10^{10}	2.87×10^{10}	2.82×10^{10}
μ_1	1.16×10^{4}	2.00×10^{4}	3.35×10^{4}
β_1	7.96×10	2.01×10^{2}	3.56×10^{2}
β_2	-2.92×10^{-7}	-9.91×10^{-8}	-1.39×10^{-7}
$V_t^{1/2}$	3.52×10^{-3}	6.99×10^{-3}	7.89×10^{-3}

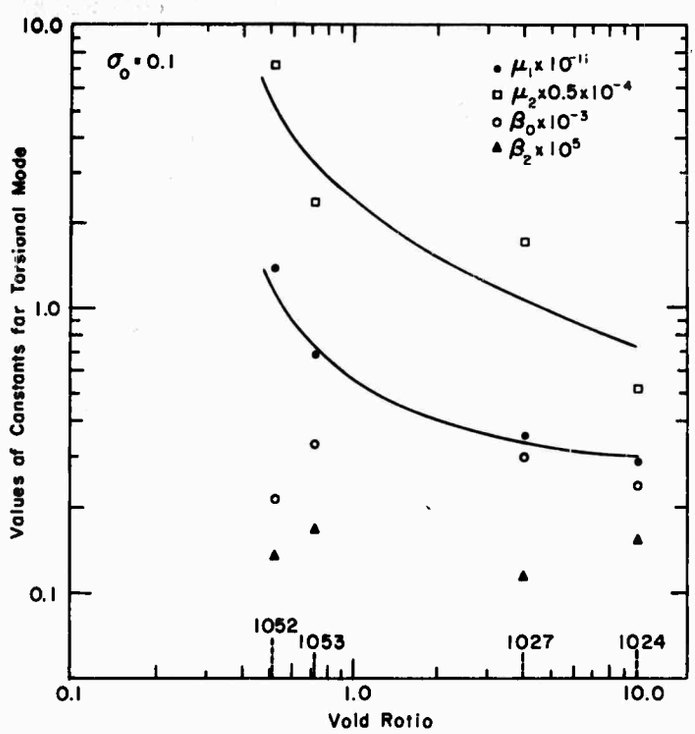

Figure 10. Values of constants for torsional mode vs void ratio.

In this case σ_{xx} is the applied stress and the other five components of stress are zero. The first three equations in eq 9 thus become:

$$(R + S)\,\sigma_{xx} = P\Delta + 2Q\epsilon_{xx} \tag{25a}$$

$$R\,\sigma_{xx} = P\Delta + 2Q\epsilon_{yy} \tag{25b}$$

$$R\,\sigma_{xx} = P\Delta + 2Q\epsilon_{zz}. \tag{25c}$$

Eliminating ϵ_{yy} and ϵ_{zz} from eq 25, we obtain the following equation:

$$[Q(R + S) + PS]\,\sigma_{xx} = (3PQ + 2Q^2)\,\epsilon_{xx}. \tag{26}$$

The operators Q and S have been determined and the operators P and R are now to be determined from the longitudinal vibration tests. The determination of P and R is more elaborate than the determination of Q and S, since restrictions have already been imposed on the former in relation to the latter.

We intend to introduce four new parameters to define P and Q. There are several ways of choosing such parameters. In the general constitutive relation, eq 9, if all other constants except λ_1, μ_1 and β_1 are vanishing and β_1 is equal to unity as already defined, eq 9 reduces to the elastic constitutive equation, or Hooke's law in terms of an incremental strain resulting in an incremental stress, where λ_1 and μ_1 are Lamé constants. It is anticipated that the dynamic properties of frozen soils do not deviate markedly from those of an elastic solid. Thus the parameter λ_1 is expected to play an important role in the operator P. We choose two models defined by two four-parameter groups, $(\lambda_0, \lambda_1, a_1, a_2)$ and $(\lambda_1, \lambda_2, a_1, a_2)$. Now we have

$$P = \lambda_0 + \lambda_1 \frac{\partial}{\partial t} + \lambda_2 \frac{\partial^2}{\partial t^2} \tag{27a}$$

$$R = a_1 \frac{\partial}{\partial t} + a_2 \frac{\partial^2}{\partial t^2} \tag{27b}$$

where $\lambda_2 = 0$ for Model 1 and $\lambda_0 = 0$ for Model 2.

When σ_{xx} and ϵ_{xx} are harmonic with an angular frequency ω, then the complex Young's modulus E is given as,

$$E = \frac{M}{L} = \frac{M_1 + iM_2}{L_1 + iL_2} \tag{28}$$

where

$$L_1 = -\mu_1\omega a_1 + \mu_2\omega^3 a_2 - \omega(\mu_1\beta_1 + \mu_2\beta_0 + \lambda_1\beta_1 + \lambda_2\beta_0) + \omega^3(\mu_2\beta_2 + \lambda_2\beta_2) + \lambda_0(\beta_0 - \beta_2\omega^2)/\omega \tag{29a}$$

$$L_2 = -\mu_2\omega^2 a_1 - \mu_1\omega^2 a_2 + \beta_0\mu_1 + \lambda_1\beta_0 + \lambda_0\beta_1 - \omega^2(\mu_1\beta_2 + \mu_2\beta_1 + \lambda_1\beta_2 + \lambda_2\beta_1) \tag{29b}$$

$$M_1 = -\omega(3\lambda_1\mu_1 + 2\mu_1^2 + 3\lambda_0\mu_2) + \omega^3(3\lambda_2\mu_2 + 2\mu_2^2) \tag{29c}$$

$$M_2 = 3\lambda_0\mu_1 - \omega^2(3\lambda_1\mu_2 + 3\lambda_2\mu_1 + 4\mu_1\mu_2). \tag{29d}$$

Knowing the values of μ_1, μ_2, β_0 and β_2, we determine two groups of four unknown constants, $(\lambda_0, \lambda_1, a_1, a_2)$ and $(\lambda_1, \lambda_2, a_1, a_2)$ from the observed complex modulus and the observed loss factor at any two distinct frequencies by a method similar to that used for the torsional mode. Finally we select one of the groups, which minimizes the error V_l, defined as:

$$V_l = \frac{[(E^{(1)} - E_m^{(1)})^2 + (E^{(2)} - E_m^{(2)})^2]}{(E^{(1)2} + E^{(2)2})} \tag{30}$$

where $E^{(i)}$, $E_m^{(i)}$ are defined as in torsional vibration. The phase velocity V_{lp} and the group velocity V_{lg} are given as for the torsional mode:

$$V_{lp} = \sqrt{\frac{E^*}{\rho}} \sec\left(\frac{\delta_l}{2}\right) \tag{31a}$$

$$V_{lg} = \frac{\sqrt{\frac{E^*}{\rho}}}{\cos\frac{\delta_1}{2} - \frac{\omega}{2}\frac{E^*_\omega}{E^*}\cos\frac{\delta_1}{2} - \frac{\omega}{2}\delta_{1\omega}\sin\frac{\delta_1}{2}} \tag{31b}$$

where

$$E^* = |E|$$

$$\delta_1 = \tan^{-1}\frac{E_2}{E_1}$$

$$E^*_\omega = \frac{\partial E^*}{\partial \omega}$$

$$\delta_{1\omega} = \frac{\partial \delta_1}{\partial \omega}$$

$$E_1 = \mathrm{Re}(E)$$

$$E_2 = \mathrm{Im}(E).$$

Results and discussion. The actual computation of four parameters, either (λ_0, λ_1, a_1, a_2) or (λ_1, λ_2, a_1, a_2), was made in the same way as in the torsional mode. We used the observed modulus and the loss factors at 1.00 kHz and 2.00 kHz. It turns out that Model 1 always gives a better approximation than Model 2 for all ice-saturated frozen soils examined. The results of the computation are shown in Table III. The degree of approximation is not satisfactory. The values of $V_t^{1/2}$ vary in the range of $10^{-2} \sim 10^{-1}$, which is much larger than $V_t^{1/2}$. It might be possible to obtain a better or well balanced approximation for both torsional and longitudinal modes by selecting eight parameters in a different manner. Also one could improve accuracy by introducing more parameters.

The most commonly used linear viscoelastic models for earth media have been the Maxwell or Voigt models with only two parameters and very little attention has been directed toward examination of the complete constitutive equation. Although the dynamic behavior of frozen soils is less complex than that of unfrozen soils, the degree of deviation from perfect elasticity is surprisingly large. It is felt that further efforts should be made to investigate the constitutive equation of frozen earth materials according to the theory of continua.

Table III. Values of constants for longitudinal mode.

(1) SN 1053 Manchester Silt

σ_0	0.1	1.0	5.0
λ_0	-4.28×10^{15}	-4.28×10^{15}	-4.71×10^{15}
λ_1	7.05×10^{10}	7.60×10^{10}	7.82×10^{10}
α_1	6.50×10^{-1}	6.52×10^{-1}	7.89×10^{-1}
α_2	1.53×10^{-4}	1.53×10^{-4}	1.82×10^{-4}
$V_t^{1/2}$	1.41×10^{-1}	1.41×10^{-1}	1.76×10^{-1}

(2) SN 1052 Ottawa Sand

σ_0	0.1	1.0	5.0
λ_0	1.50×10^{14}	1.41×10^{14}	1.33×10^{14}
λ_1	4.80×10^{10}	4.52×10^{10}	4.21×10^{10}
α_1	-1.92×10^{-1}	3.21×10^{-2}	5.65×10^{-2}
α_2	1.87×10^{-6}	2.39×10^{-6}	3.83×10^{-6}
$V_t^{1/2}$	1.18×10^{-1}	1.10×10^{-1}	1.02×10^{-1}

(3) SN 1027 Fairbanks Silt

σ_0	0.1	1.0	5.0
λ_0	-1.44×10^{15}	-7.18×10^{14}	-1.01×10^{15}
λ_1	4.37×10^{10}	3.73×10^{10}	9.13×10^{10}
α_1	1.77×10^{-1}	-7.04×10^{-2}	5.58×10^{-1}
α_2	4.40×10^{-5}	1.28×10^{-5}	2.35×10^{-5}
$V_t^{1/2}$	6.64×10^{-2}	3.78×10^{-2}	8.37×10^{-2}

(4) SN 1024 Polycrystalline Ice

σ_0	0.1	1.0	5.0
λ_0	4.26×10^{14}	1.91×10^{14}	4.60×10^{14}
λ_1	4.58×10^{10}	4.56×10^{10}	4.79×10^{10}
α_1	-6.75×10^{-1}	-5.37×10^{-1}	-2.35×10^{0}
α_2	1.36×10^{-5}	3.70×10^{-6}	9.41×10^{-5}
$V_t^{1/2}$	1.32×10^{-1}	8.35×10^{-2}	1.22×10^{-1}

(5) SN 1023 Polycrystalline Ice

σ_0	0.1	1.0	5.0
λ_0	3.82×10^{14}	4.38×10^{14}	3.05×10^{14}
λ_1	4.69×10^{10}	4.69×10^{10}	4.34×10^{10}
α_1	-5.73×10^{-1}	-7.01×10^{-1}	-1.39×10^{0}
α_2	3.31×10^{-6}	7.55×10^{-6}	5.44×10^{-6}
$V_t^{1/2}$	6.65×10^{-2}	1.02×10^{-1}	4.67×10^{-1}

Literature Cited

Eringen, A.C. (1967) *Mechanics of continua*. New York: John Wiley and Sons.

Hardin, B.O. and F.E. Richart (1963) Elastic wave velocities in granular soils. *Journal of Soil Mechanics Foundations Division ASCE*, vol. 89, p. 33-65.

Hardin, B.O. (1965) The nature of damping in sands. *Journal of Soil Mechanics Foundations Division ASCE*, vol. 91, p. 55-74.

Hardin, B.O. and W.A. Mossbarger (1966) The resonant column technique for vibration testing of soils and asphalts. *Proceedings Instrument Society of America.*

Hardin, B.O. and W.L. Black (1968) Vibration modulus of normally consolidated clay. *Journal of Soil Mechanics Foundations Division ASCE*, vol. 94, p. 353-369.

Literature Cited (Cont'd)

Hardin, B.O. and V.P. Drnevich (1970) Shear modulus and damping in soils, I. Measurement and parameter effect, II. Design equations and curves. Tech. Rep. UKY 27-70-CE 2 and 3, University of Kentucky.

Jackson, D.D. and D.L. Anderson (1970) Physical mechanisms of seismic-wave attenuation. *Reviews Geophysics Space Physics*, vol. 8, p. 1-63.

Lee, T.M. (1963) Method of determining dynamic properties of viscoelastic solids employing forced vibration. *Journal of Applied Physics*, vol. 34, p. 1524-1529.

Norris, D.M., Jr. and Wun-Chung Young (1970) Longitudinal forced vibration of viscoelastic bars with end mass. U.S. Army Cold Regions Research and Engineering Laboratory (USA CRREL) Special Report no. 135.

Stevens, H. et al. (1967) Hugoniot and dynamic properties of frozen earth materials. Final Report to ARPA prepared under ARPA order 968.

Simmons, G. and W.F. Brace (1965) Comparison of static and dynamic measurements of compressibility of rocks. *Journal of Geophysical Research*, vol. 70, p. 5649-5656.

Thurston, R.N. (1964) Wave propagation in fluids and normal solids. In the book Physical Acoustics, vol. I, Part A, edited by Mason, W.P. Academic Press.

Volarovich, M.P. and A.S. Gurvich (1957) Investigation of dynamic moduli of elasticity for rocks in relation to temperature. Bull. Acad. Sci. USSR, Geophys. Ser., 1957, 1.

III. THE USE OF FREE OSCILLATIONS TO MEASURE THE ELASTIC PROPERTIES OF MATERIALS

by

M. Smith, R. Martin, and Y. Nakano

Introduction

This section discusses our efforts to develop, and apply, experimental techniques for the measurement of the elastic and slightly anelastic properties of materials based on the free resonances of layered elastic spheres. We initially undertook this effort because such spheres are the only bounded bodies, known to us, for which we could develop exact analytic solutions. Consequently we are not, *a priori*, restricted to considering only high or low frequency approximations or time-limited response.

Although some classic studies of the dynamic properties of elastic spheres have long been available (see Love, 1944), the results were generally devoid of practical significance until the Earth's free oscillations were observed after the Chilean earthquake of 1960 (Bullen, 1963). The consequent attention by seismologists resulted in a well-developed literature from which many of our references are drawn. We differ slightly in that we restrict our attention to spheres composed of discrete layers and we also neglect the effects of self-gravitation, rotation, an initial stress state, and ellipticity (see Dahlen, 1968).

The following three sections and the appendices are theoretical, with some numerical examples. So far as we are aware, the particular development given here, that is, a layered non-gravitating sphere, has not been published, of a piece, elsewhere. It is, however, a "standard," albeit complicated, problem. We believed that its detailed solution had to be explicitly laid down before progressing into experiment.

The last sections deal with the results of pilot experimentation. We believe the results indicate that the practical difficulties associated with this method are being mastered and that the technique is a viable one.

Elastic Displacement Solutions in Spherical Coordinates

We consider a volume of space filled with an isotropic, homogeneous, linearly elastic medium having Lamé constants λ and μ, and density ρ. We assume the medium to be free of gravitation and other body forces, but allow the existence of one of more surfaces across which tractions may be applied.

Let $\mathbf{u}$ be the displacement field specifying the motion of each particle from its unique rest position. We assume $\mathbf{u}$ to be a first order infinitesimal and do not, therefore, have to distinguish

between Eulerian and Lagrangian coordinate systems. Let $\underline{T}$ be the elastic stress tensor. If we assume that $\mathbf{u} = 0$ corresponds with the unstressed state of the medium, $\underline{T}$ is given by (Fung, 1965)

$$\underline{T} = \lambda(\nabla \cdot \mathbf{u})\underline{I} + \mu(\nabla\mathbf{u} + \mathbf{u}\nabla), \tag{1}$$

where $\underline{I}$ is the identity tensor. $\nabla\mathbf{u}$ is the gradient tensor of $\mathbf{u}$, and $\mathbf{u}\nabla$ is its transpose.

The conservation of linear momentum leads immediately to the equation of motion,

$$\rho\partial_t^2\mathbf{u} = \nabla \cdot \underline{T}. \tag{2}$$

Equation 1 and some standard vector calculus identities convert eq 2 to

$$\rho\partial_t^2\mathbf{u} = (\lambda + 2\mu)\nabla(\nabla \cdot \mathbf{u}) - \mu\nabla \times \nabla \times \mathbf{u}. \tag{3}$$

We choose to represent $\mathbf{u}$ by

$$\mathbf{u} = \vec{r}U + \nabla_1 V - \vec{r} \times \nabla_1 W \tag{4}$$

where U, V, and W are scalar fields and ∇_1 is defined by

$$\nabla_1 = \vec{\theta}\partial_\theta + \vec{\phi}(\sin\theta)^{-1}\partial\phi. \tag{5}$$

$\vec{r}$ is a unit vector directed away from the origin, θ and ϕ are the colalitude and longitude, and $\vec{\theta}$ and $\vec{\phi}$ are their respective unit vectors. ∇_1 is the gradient operator on the surface of a sphere of unit radius. It is related to the three-dimensional gradient by

$$\nabla = \vec{r}\partial_r - r^{-1}\nabla_1. \tag{6}$$

After some algebra, we can show (Backus, 1967) that

$$\nabla(\nabla \cdot \mathbf{u}) = \vec{r}\partial_r\left\{\left(\partial_r + \frac{2}{r}\right)U + r^{-1}\nabla_1^2 V\right\} + \nabla_1\left\{\left(r^{-1}\partial_r + \frac{2}{r^2}\right)U + r^{-2}\nabla_1^2 V\right\}, \tag{7}$$

and

$$\nabla \times \nabla \times \mathbf{u} = \vec{r}\{r^{-2}\partial_r(r\nabla_1^2 V) - r^{-2}\nabla_1^2 U\} + \nabla_1\{r^{-1}\partial_r U - r^{-1}\partial_r^2(rV)\} + \vec{r} \times \nabla_1\{r^{-2}\nabla_1^2 W + r^{-1}\partial_r^2(rW)\}. \tag{8}$$

We insert eq 4, 7 and 8 into eq 3. We now appeal to the uniqueness of the representation 4 (Backus, 1967) to yield the three coupled partial differential equations

$$\rho \partial_t^2 U = (\lambda + 2\mu)\partial_r \left\{ \left(\partial_r + \frac{2}{r} \right) U + r^{-1} \nabla_1^2 V \right\} -$$

$$- \frac{\mu}{r^2} \left\{ \partial_r (r \nabla_1^2 V) - \nabla_1^2 U \right\}, \tag{9a}$$

$$\rho \partial_t^2 V = (\lambda + 2\mu) \left\{ \left(r^{-1} \partial_r + \frac{2}{r^2} \right) U + r^{-2} \nabla_1^2 V \right\} -$$

$$- \frac{\mu}{r} \left\{ \partial_r U - \partial_r^2 (rV) \right\}, \tag{9b}$$

and

$$\rho \partial_t^2 W = \frac{\mu}{r} \left\{ \partial_r^2 (rW) + r^{-1} \nabla_1^2 W \right\}. \tag{9c}$$

We note that both V and W may be augmented by any constant without affecting $\mathbf{u}$ (see eq 4). Therefore, we may expect these two scalar fields to be determined only to within an additive constant. We also note that eq 9a and 9b both involve U and V but not W, while eq 9c involves W but neither of U and V.

The manner in which one elects to solve eq 9a, 9b and 9c (plus whatever boundary conditions appertain) depends upon the intended application of the solution. For our purposes, we wish to find a set of complete, linearly independent vector fields $\{\mathbf{f}^1, \mathbf{f}^2, \ldots\}$ each of which satisfies eq 3. If the set is complete, all possible solutions to eq 3 may then be expressed as some linear combination of the members of the set, the coefficients used in the expansion being determined by boundary and initial conditions.

In pursuit of this, we Fourier transform eq 9a-9c, going from time t to angular frequency ω. We do not introduce a distinct symbol for Fourier transforms since it will be clear from the context whether a symbol refers to the transformed or untransformed variable. The result of Fourier transformation is to replace ∂_t^2 by $-\omega^2$.

To transform the resultant trio of equations from partial to ordinary differential equations we introduce a surface spherical harmonic expansion of U, V and W. For $l \geq 0$ and $-l \leq m \leq l$, we define (Hill, 1953)

$$Y_l^m(\theta, \phi) = (-1)^m \left[\frac{2l + 1}{4\pi} \frac{(l - |m|)!}{(l + |m|)!} \right]^{1/2} P_l^m(\cos\theta)\, e^{im\phi} \tag{10}$$

where P_l^m is the Associated Legendre Function given by

$$P_l^m(x) = \frac{(1 - x^2)^{(|m|/2)}}{2^l l!} \partial_x^{l+|m|} (x^2 - 1)^l. \tag{11}$$

If S_1 is the surface of a sphere of unit radius centered on the origin, the Y_l^m are orthonormal in the sense

$$\int_{S_1} Y_l^m(\theta, \phi)\, \overline{Y_\lambda^\mu(\theta, \phi)} \sin\theta d\theta d\phi = \delta_{l\lambda}\delta_{m\mu} \tag{12}$$

where the bar indicates complex conjugation and δ_{ij} is the Kronecker delta.

The $Y_l^m(\theta, \phi)$ form a complete set and, if we assume U, V and W are sufficiently regular, we may expand them as

$$U(r, \theta, \phi, \omega) = \sum_{l=0}^{\infty} \sum_{m=-l}^{l} U_l^m(r, \omega) Y_l^m(\theta, \phi), \tag{13a}$$

$$V(r, \theta, \phi, \omega) = \sum_{l=1}^{\infty} \sum_{m=-l}^{l} V_l^m(r, \omega) Y_l^m(\theta, \phi), \tag{13b}$$

and

$$W(r, \theta, \phi, \omega) = \sum_{l=1}^{\infty} \sum_{m=-l}^{l} W_l^m(r, \omega) Y_l^m(\theta, \phi). \tag{13c}$$

The $l = 0$ terms have been omitted from eq 13b and 13c since inspection of eq 4 reveals that these terms do not contribute to the displacement field.

We now insert eq 13a-13c into the transformed equations 9a-9c, and make use of the relation

$$\nabla_1^2 Y_l^m = -l(l+1) Y_l^m. \tag{14}$$

The resultant expressions are then multiplied by a particular Y_l^m and integrated over the surface of a sphere of radius r. Application of eq 12 leads immediately to

$$-\rho\omega^2 U_l^m = (\lambda + 2\mu)\partial_r \left\{\left(\partial_r + \frac{2}{r}\right) U_l^m - \frac{l(l+1)}{r} V_l^m\right\} + \frac{\mu}{r^2}\{l(l+1)\partial_r(rV_l^m) - l(l+1)U_l^m\} \tag{15a}$$

$$-\rho\omega^2 V_l^m = (\lambda + 2\mu)\left\{\left(r\partial_r + \frac{2}{r^2}\right) U_l^m - \frac{l(l+1)}{r^2} V_l^m\right\} - \frac{\mu}{r}\{\partial_r U_l^m - \partial_r^2(rV_l^m)\}, \tag{15b}$$

and

$$-\rho\omega^2 W_l^m = \frac{\mu}{r}\left\{\partial_r^2(rW_l^m) - \frac{l(l+1)}{r} W_l^m\right\}. \tag{15c}$$

We note that none of eq 15a-15c explicitly involves m.

The set 15a-15c can be solved by any of several standard techniques. The method used here is detailed in Appendix A. The results are

$$\begin{Bmatrix} U_l \\ V_l \end{Bmatrix} = \begin{Bmatrix} \partial_r j_l(kr) & \dfrac{l(l+1)}{r} j_l(\gamma r) & \partial_r y_l(kr) & \dfrac{l(l+1)}{r} y_l(\gamma r) \\ \dfrac{j_l(kr)}{r} & r^{-1}\partial_r [r j_l(\gamma r)] & \dfrac{y_l(kr)}{r} & r^{-1}\partial_r [r j_l(\gamma r)] \end{Bmatrix} \begin{Bmatrix} A_l \\ B_l \\ C_l \\ D_l \end{Bmatrix} \quad \text{for } l > 0; \tag{16}$$

$$U_0 = \{\partial_r j_0(kr) \quad \partial_r y_0(kr)\} \begin{Bmatrix} A_0 \\ C_0 \end{Bmatrix} \tag{17a}$$

and

$$V_0 = 0; \tag{17b}$$

$$W_l = \{r j_l(\gamma r) \quad r y_l(\gamma r)\} \begin{Bmatrix} E_l \\ F_l \end{Bmatrix} \quad \text{for } l > 0; \tag{18a}$$

$$W_0 = 0; \tag{18b}$$

where

$$k = \frac{\omega}{\sqrt{\dfrac{(\lambda + 2\mu)}{\rho}}} = \frac{\omega}{V_p}, \tag{19}$$

and

$$\gamma = \frac{\omega}{\sqrt{\dfrac{\mu}{\rho}}} = \frac{\omega}{V_s}. \tag{20}$$

V_p and V_s are, respectively, the compressional and shear velocities of the medium. Each of A_l, B_l, ..., F_l represents a spherical harmonic of degree l. That is, each one is some linear combination of the $2l + 1$ functions $\{Y_l^{-l}, \ldots, Y_l^0, \ldots, Y_l^l\}$ but we cannot specify, without considering a particular problem, *what* linear combination each is. To be specific, we may express them as

$$A_l(\theta, \phi) = \sum_{m=-l}^{l} A_l^m Y_l^m(\theta, \phi), \tag{20a}$$

and similarly for B_l, C_l, D_l, E_l and F_l. The $A_l \ldots$ are *not* constants but the $A_l^m \ldots$ are. Equations 16-18 thus contain $6(2l + 1)$ presently undetermined constants. (When $l = 0$, there are only two constants.)

We believe that the manner in which we have dealt with the spherical harmonics merits further elaboration. We will use eq 19 as an example. We could retain the superscript m and have

$$W_l^m = \{E_l^m r j_l(\gamma r) + F_l^m r y_l(\gamma r)\} Y_l^m(\theta, \phi). \tag{21}$$

Let us then define

$$W_l = \sum_{m=-l}^{l} W_l^m .$$

Combining these, we have

$$W_l = r j_l(\gamma r) \sum_{m=-l}^{l} E_l^m Y_l^m(\theta, \phi) + r y_l(\gamma r) \sum_{m=-l}^{l} F_l^m Y_l^m(\theta, \phi)$$

where we were able to regroup the sums because each of the two independent solutions to eq 15c, namely $r j_l(\gamma r)$ and $r y_l(\gamma r)$, is independent of m. This last expression is simply eq 18a.

Any linear combination of spherical harmonics of the form

$$H_l = \sum_{m=-l}^{l} a_l^m Y_l^m(\theta, \phi) \tag{22}$$

is itself a spherical harmonic and satisfies

$$\nabla_1^2 H_l = -l(l+1) H_l . \tag{23}$$

The set $\{Y_l^{-l}, \ldots, Y_l^0, \ldots, Y_l^l\}$ serves only as an orthonormal basis for the $2l + 1$ dimensional space of spherical harmonics satisfying eq 22, and has no inherent significance. At this point in our development we can only know, then, that each set of radial functions in eq 16-18 will be multiplied by some spherical harmonic, H_l. We cannot know H_l's precise form; the a_l^m in eq 22 will be determined by boundary and initial conditions.

Free Oscillations of a Layered Elastic Sphere

We consider a sphere divided into N concentric spherical shells. We number the shells from the center outwards and let r_i be the outermost radius of the i^{th} shell. Then r_N is the radius of the sphere. Let r_0 equal zero. We suppose that the i^{th} shell is composed of an elastic, homogeneous, isotropic medium of density ρ_i and having Lamé parameters λ_i and μ_i. These parameters define the compressional velocity V_{pi} and the shear velocity V_{si}.

We assume that the surface $r = r_N$ is free from all tractions, and that no body forces (such as gravitation) are present. We wish to know for what angular frequencies ω there exists a non-trivial displacement $\mathbf{u}(\mathbf{r})\, e^{i\omega t}$, such that the surface is free of traction and all internal boundary conditions (discussed below) are fulfilled. We shall label such angular frequencies *eigenfrequencies* and their associated displacements *eigenfunctions*. We refer to such traction-free motions as *free oscillations*.

Let $\mathbf{u}^{(i)}(\mathbf{r})\, e^{i\omega t}$ be the displacement field in the layer. From the displacement, we can compute a stress tensor, $\underline{T}^{(i)}$, by eq 1. Equation 2, namely,

$$\rho \partial_t^2 \mathbf{u} = \nabla \cdot \underline{T} \tag{2}$$

must hold everywhere in the medium, since it expresses only the conservation of momentum and is not dependent upon such assumptions as isotropy, homogeneity, etc. In particular, eq 2 is valid

in a small "Gaussian pillbox" which encompasses a portion of the surface $r = r_i$, the boundary between the i^{th} and $(i + 1)^{th}$ shells. Let ν denote the volume enclosed between the radii $r_i - \delta r$ and $r_i + \delta r$ and by some range of the coordinates θ and ϕ. Then

$$\int_\nu \rho \partial_t^2 \mathbf{u} d\nu = \int_\nu \nabla \cdot \underline{T} d\nu. \tag{24}$$

If Σ is the surface of ν, Gauss's theorem leads to

$$\int_\nu \rho \partial_t^2 u d\nu = \int_\Sigma \underline{T} \cdot \vec{n} d\sigma$$

where $\mathbf{n}$ is the unit outward normal on Σ. If we let δr go to zero, then the volume of ν also vanishes and, if $\rho \partial_t^2 \mathbf{u}$ remains bounded, the left-hand integral goes to zero. The right-hand side becomes

$$\int_\Sigma \{\underline{T}^{(i+1)} - \underline{T}^{(i-1)}\} \cdot \vec{r} d\sigma = 0 \quad \text{at } r = r_i. \tag{25}$$

Since this result is independent of the details of the shape of Σ we conclude that the quantity $\underline{T} \cdot \vec{r}$ must be everywhere continuous, and in particular across boundaries.

To condition 25 we add one expressing our intuition of the behavior of elastic materials. If both the i^{th} and $(i + 1)^{th}$ shells are solid, we require that the displacement $\mathbf{u}$ be continuous. We refer to interfaces at which this is true as being "welded." If, however, one or both shells are fluid (that is, $\mu = 0$), we require only the radial component of displacement to be continuous. In the latter case, we allow the boundary to slip but in neither case do we allow holes to open or matter to interpenetrate itself.

The quantity $\underline{T} \cdot \vec{r}$ is a vector and represents the traction (force) acting on a surface normal to $\vec{r}$. In a fashion identical to eq 4, we may represent it as

$$\underline{T} \cdot \vec{r} = \vec{r} P + \nabla_1 Q - \vec{r} \times \nabla_1 R, \tag{26}$$

where P, Q and R are scalar fields. Equation 25 states that P, Q and R are continuous across an interface. The stress-displacement relations, eq 1, enable us to relate P, Q and R to U, V and W, the scalar representatives for $\mathbf{u}$. These relations, which are derived in Appendix B, are

$$P = (\lambda + 2\mu)\partial_r U + \frac{2\lambda}{r} U + \frac{\lambda}{r} \nabla_1^2 V, \tag{27a}$$

$$Q = \mu \left\{ \frac{U}{r} + r \partial_r \left(\frac{V}{r} \right) \right\}, \tag{27b}$$

and

$$R = \mu r \partial_r \left(\frac{W}{r} \right). \tag{27c}$$

The import of the boundary conditions, then, is that P, Q, R and U are continuous everywhere and V and W are continuous in solid domains.

We now have six scalar fields to contend with. However, an examination of eq 16, 17, 18 and 27 indicates that we can group them into two sets, one consisting of U, V, P and Q, and one consisting of W and R. These two sets are completely independent; they do not interact in any way. And we may, without loss of generality, treat them separately.

The set (U, V, P, Q) is the set of *spheroidal* variables. The displacements described by this set give rise to both compressional and shear strain, and are interference products of compressional and vertically polarized shear waves. Among other things, this set gives rise to the spherical type of Rayleigh surface waves.

The set (W, R) is the set of *toroidal* variables. The displacements described by this set are orthogonal to r and produce only shear strains. They are the interference products of horizontally polarized shear waves. Love surface waves are associated with this set.

From this point forward we will discuss only spheroidal types of motion. A similar development for toroidal oscillations can be easily formulated since the toroidal problem is, in fact, substantially simpler.

For any specified angular frequency of oscillation ω, the set (U, V, P, Q) can be expanded in terms of spherical harmonics as

$$U(r, \theta, \phi, \omega) = \sum_{l=0}^{\infty} \sum_{m=-l}^{l} U_l^m(r, \omega)\, Y_l^m(\theta, \phi) \tag{13a}$$

$$V(r, \theta, \phi, \omega) = \sum_{l=1}^{\infty} \sum_{m=-l}^{l} V_l^m(r, \omega)\, Y_l^m(\theta, \phi) \tag{13b}$$

$$P(r, \theta, \phi, \omega) = \sum_{l=0}^{\infty} \sum_{m=-l}^{l} P_l^m(r, \omega)\, Y_l^m(\theta, \phi) \tag{28a}$$

$$Q(r, \theta, \phi, \omega) = \sum_{l=1}^{\infty} \sum_{m=-l}^{l} Q_l^m(r, \omega)\, Y_l^m(\theta, \phi). \tag{28b}$$

The U_l^m and V_l^m are given, in terms of a set of coefficients, by the analytic solutions 16 and 17. P_l^m and Q_l^m are then given by eq 27. Our problem is to determine those frequencies, ω, for which we can construct U, V, P and Q by this method, for each layer, such that all boundary and interface conditions are met.

However, because the Y_l^m are an orthogonal set, we may consider the above problem separately for each Y_l^m. That is, given

$$U(r, \theta, \phi, \omega) = U_l^m(r, \omega)\, Y_l^m(\theta, \phi), \tag{29}$$

etc., for what angular frequencies ω can we satisfy all internal and external boundary conditions? Since m, as discussed earlier, is a degenerate index, we can simplify eq 29 to

$$U(r, \theta, \phi, \omega) = U_l(r, \omega)\, H_l(\theta, \phi), \tag{30a}$$

$$V(r, \theta, \phi, \omega) = V_l(r, \omega)\, H_l(\theta, \phi), \tag{30b}$$

$$P(r, \theta, \phi, \omega) = P_l(r, \omega) H_l(\theta, \phi), \tag{30c}$$

and

$$Q(r, \theta, \phi, \omega) = Q_l(r, \omega) H_l(\theta, \phi), \tag{30d}$$

where H_l is given by eq 22 and is some spherical harmonic of degree l. The details of H_l are of no particular interest since the eigenfrequencies and the form of $U_l, \ldots, Q_l$ remain fixed no matter what H_l we choose.

Our problem now is to find the eigenfrequencies associated with spherical harmonics of degree l. If we wish to know all eigenfrequencies, we must repeat this procedure for each of $l = 0, 1, 2, \ldots$

We will devise a constructive algorithm which will enable us, for a given angular frequency ω, to construct a solution from the center outward which meets all boundary conditions save one. If the last condition is met, ω is then an eigenfrequency.

We consider eq 16, which expressed U_l and V_l as a linear combination of four independent functions of radius. The coefficients $A_l, \ldots, D_l$ were taken to incorporate all spherical harmonic content. Equation 27 allows us to extend eq 16 to

$$\begin{Bmatrix} U_l^i \\ V_l^i \\ P_l^i \\ Q_l^i \end{Bmatrix} = \underline{H}_l^i \begin{Bmatrix} A_l^i \\ B_l^i \\ C_l^i \\ D_l^i \end{Bmatrix} \tag{31}$$

where $i = 1, \ldots, N$ designates the layer to which the solution is appropriate. $\underline{H}_l^i$ is a 4×4 matrix constructed from

$$h_{3j} = (\lambda + 2\mu)\, \partial_r h_{1j} + \frac{2\lambda}{r} h_{1j} - \lambda \frac{l(l+1)}{r} h_{2j}, \tag{32a}$$

and

$$h_{4j} = \mu \{ r^{-1} h_{1j} + r\, \partial_r (r^{-1} h_{2j}) \} \tag{32b}$$

and the first two rows of $\underline{H}_l^i$ are taken from eq 16. The set $\{A_l^i, \ldots D_l^i\}$ serve as constants, and not spherical harmonics. For the remainder of this development, we shall omit the θ and ϕ terms for convenience.

We rewrite eq 31 as

$$\mathbf{S}^i(r) = \underline{H}^i(r) \cdot \mathbf{C}^i \tag{33}$$

where we have omitted the subscript l. The vector $\mathbf{S}^i(r)$ includes both the stress and displacement terms.

We will now proceed to construct a solution satisfying all internal boundary conditions. In region 1 which includes the point $r = 0$ we can *a priori* eliminate those solutions which go as $y_1(kr)$ and $y_1(\gamma r)$. Therefore, $\mathbf{C}^1$ has the form

$$\mathbf{C}^1 = \begin{Bmatrix} A^1 \\ B^1 \\ 0 \\ 0 \end{Bmatrix} = A^1\vec{e}_1 + B^1\vec{e}_2 \tag{34}$$

where $\vec{e}_1$ and $\vec{e}_2$ are four-dimensional unit coordinate vectors directed along the first and second coordinate axes. In the first region, then, we have

$$\mathbf{S}^1(r) = \underline{H}^1(r) \cdot \{A^1\vec{e}_1 + B^1\vec{e}_2\}. \tag{35}$$

In the second region, we have

$$\mathbf{S}^2(r) = \underline{H}^2(r) \cdot \mathbf{C}^2. \tag{36}$$

Assuming both regions to be solid, the boundary conditions require that

$$\mathbf{S}^2(r_1) = \mathbf{S}^1(r_1), \tag{37}$$

or

$$\underline{H}^2(r_1) \cdot \mathbf{C}^2 = \underline{H}^1(r_1) \cdot \{A^1\vec{e}_1 + B^1\vec{e}_2\}. \tag{38}$$

Because the solution composing the columns of $\underline{H}$ is linearly independent, matrix theory guarantees that $\underline{H}$ is nonsingular. Therefore, we may express $\mathbf{C}^2$ as

$$\mathbf{C}^2 = [\underline{H}^2(r_1)]^{-1} \cdot \underline{H}^1(r_1) \cdot \{A^1\vec{e}_1 + B^1\vec{e}_2\}. \tag{39}$$

An alternative form for eq 39 is

$$\mathbf{C}^2 = A^1\xi^2 + B^1\zeta^2 \tag{40}$$

where

$$\xi^2 = [\underline{H}^2(r_1)]^{-1} \cdot \underline{H}^1(r_1) \cdot \vec{e}_1 \tag{41}$$

$$\zeta^2 = [\underline{H}^2(r_1)]^{-1} \cdot \underline{H}^1(r_1) \cdot \vec{e}_2. \tag{42}$$

Equations 40, 41 and 42 suffice to specify $\mathbf{S}^2(r)$. By a similar procedure, we can extend the solution from the i^{th} to the $(i + 1)^{th}$ shell. The appropriate relations are

$$\mathbf{S}^{i+1}(r) = \underline{H}^{i+1}(r) \cdot \mathbf{C}^{i+1} \tag{43}$$

$$\mathbf{C}^{i+1} = A^1\xi^{i+1} + B^1\zeta^{i+1} \tag{44}$$

$$\xi^{i+1} = [\underline{H}^{i+1}(r)]^{-1} \cdot \underline{H}^i(r) \cdot \xi^i \tag{45}$$

$$\zeta^{i+1} = [\underline{H}^{i+1}(r)] \cdot \underline{H}^i(r) \cdot \zeta^i. \tag{46}$$

In fact, either of ξ^{l+1} or ζ^{l+1} can be computed alone by starting with eq 41 or 42 and simply applying eq 45 or 46 as many times as is necessary.

We suppose now that we have computed ξ^N and ζ^N where N is the number of shells. The solution in this shell is given by

$$\mathbf{S}^N(r) = \underline{H}^N(r) \cdot \{A^1 \xi^N + B^1 \zeta^N\}. \tag{47}$$

We note that both the solution associated with ξ^N [i.e., $\mathbf{S}^i(r)$ when $B^1 = 0$] and the solution associated with ζ^N separately satisfy all of the internal boundary conditions. If ω is an eigenfrequency, we will be able to find some A^1 and B^1, not both zero, such that the last two components of $\mathbf{S}^N(r_N)$ are zero.

A straightforward way to do this is to evaluate

$$^{(a)}\mathbf{S}^N = \underline{H}^N(r_N) \cdot \zeta^N, \tag{48a}$$

and

$$^{(b)}\mathbf{S}^N = \underline{H}^N(r_N) \cdot \zeta^N. \tag{48b}$$

If $\mathbf{S}_3^N(r_N)$, i.e. P, must vanish, A^1 and B^1 must satisfy

$$A^1(^aS_3^N) = - B^1(^bS_3^N). \tag{49}$$

We may, without loss of generality, impose a normalization such as

$$(A^1)^2 + (B^1)^2 = 1, \tag{50}$$

which, with eq 49, allows us to compute A^1 and B^1. Using A^1 and B^1, we then compute $S_4^N(r_N)$, i.e. Q, and examine it to see if it vanishes. If it does, ω is an eigenfrequency; if it does not, ω is not an eigenfrequency.

If ω is an eigenfrequency then we may use the values of A^1 and B^1 in eq 43 and 44 to compute the eigenfunction $\mathbf{S}^i(r)$ at any radius in the system. We recall that $\mathbf{S}^i(r)$ must be multiplied by some spherical harmonic of degree l and the factor $e^{i\omega t}$ to obtain the full solution,

$$\mathbf{S}_l^i(r, \theta, \phi, t) = \mathbf{S}_l^i(r) H_l(\theta, \phi) e^{i\omega t}$$

where we have reinstated the subscript l. We emphasize again that the precise nature of H_l depends upon initial conditions and is not relevant here.

This method requires modification when either $l = 0$ or $l \neq 0$ but one or more shells have a vanishing shear modulus. We will briefly outline the form these modifications take.

When $l = 0$, B^1 vanishes identically and only the solution is propagated. The matrix $\underline{H}_l^i$ is collapsed to a 2×2 matrix by eliminating those solutions with arguments, γr. V and Q both vanish and the only condition at $r = r_N$ is that P vanish. A^1 becomes merely a scale factor and may be taken as equal to unity.

In a fluid region, Q vanishes identically. Across a solid/fluid or fluid/fluid interface V may be discontinuous and Q is continuous and zero. If we are propagating upward through a solid and

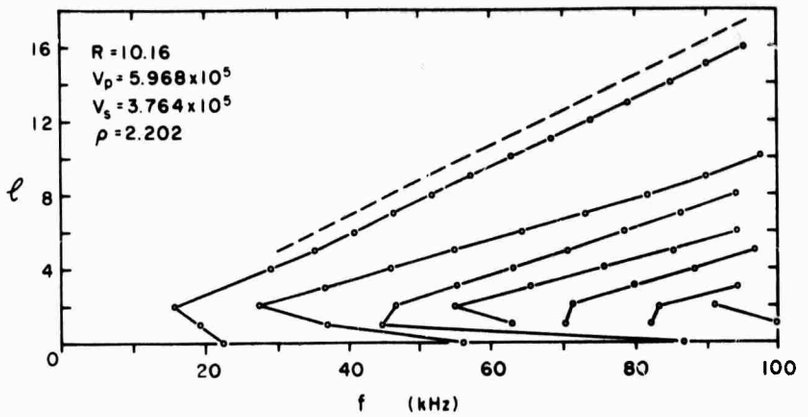

Figure 11. Loci, in the (f, l) plane, of the frequencies of free oscillation of a sphere of radius 10.16 cm composed of material having a density of 2.202 g/cm³, a compressional velocity of 5.968 × 10⁵ cm/sec, and a shear velocity of 3.764 × 10⁵ cm/sec. Solid lines connect modes of the same overtone number. Dotted line indicates the asymptotic slope (∂ω/∂l) associated with Rayleigh wave propagation in an infinite half-space having the same material properties as the sphere.

encounter a fluid, we must combine the ξ and ζ solutions to yield $Q = 0$ at the interface. This requirement determines A^1 and B^1 and, therefore, $\mathbf{C}^l$ for all shells up to, and including, the fluid region.

Consequently, in a fluid region we have only one solution. In crossing from a fluid to a solid region, we must "start" a new solution having some non-zero V, but for which U, P and Q vanish. We may always find some ζ which yields this result.

For a given l, we shall arrange the frequencies of free oscillation in ascending order, as ${}_0\omega_l$, ${}_1\omega_l$, ${}_2\omega_l$, ... We shall designate the displacements, as a function of r_1 as ${}_0\mathbf{u}_l$, ${}_1\mathbf{u}_l$, ... and the four-vector of displacement and stress by ${}_0\mathbf{S}_l$, ${}_1\mathbf{S}_l$, ..., etc. The "lowest" mode, for a given l, is referred to as the "fundamental" mode and the remainder as "overtones."

Figure 11 shows the loci, in the (ω, l) plane, of all spheroidal eigenfrequencies lying below 100 kHz for a homogeneous sphere with 10.16 cm radius. The sphere has a density of 2.202 g/cm³, a compressional velocity of 5.968 × 10⁵ cm/sec, and a shear velocity of 3.764 × 10⁵ cm/sec. The results show several features common to such calculations.

The lowest fundamental mode is ${}_0\omega_2$. This, almost always, is the case. Secondly, the modes for $l \geq 2$ tend to arrange themselves in smoothly varying suites, each of a given overtone, or radial, number. These are known to correspond to the fundamental and higher-mode Rayleigh surface waves. To establish the connection, we observe that $Y_1^l(\theta, \phi)$ has the value

$$Y_1^l(\theta, \phi) = (-1)^l \sqrt{\frac{2l+1}{4\pi(2l)!}} \frac{(\mathrm{Sm}\,\theta)^l}{2^l} e^{il\phi} \tag{51}$$

as can be seen from eq 10 and 11. Y_1^l describes motion which is closely confined to the equator ($\theta = \pi/2$) and which behaves as waves traveling circumferentially about the equatorial zone. The change of phase, per unit of distance traveled in the ϕ direction, is l/a and is therefore the mode's surface wave number. For large values of ω, we may, roughly, expect that the quantity

$$U^l = a \frac{\partial \omega}{\partial l} \tag{52}$$

represents a group velocity and

$$C^* = \frac{\omega a}{l} \tag{53}$$

represents a phase velocity. In Figure 11 we have placed a dashed line whose slope is given by eq 52 when U^* is equal to the group velocity of Rayleigh waves propagating along a half-space, the properties of which are the same as the sphere's. We regard the agreement as good.

The numerical techniques used in this, and subsequent, calculations are discussed in Appendix C.

The Inverse Problem

In the preceding two sections we have developed the "forward" problem for a layered elastic sphere. The forward problem consists of the generation of the eigenvalue spectrum associated with a given model. In this section we consider the inverse problem of utilizing a measured eigenvalue spectrum (which will, inevitably, be incomplete) to infer the properties of the materials of which the sphere is composed.

Let M be the space of all layered elastic spheres having N layers delimited by the points $\{r_0, r_1, \ldots, r_N\}$ where, as before, $r_0 = 0$ and r_N is the sphere's radius. Then all models in M have a common geometry but differ in the elastic properties (including density) of their component shells. M, then, is a space of dimension $3N$ (since each shell has three distinct properties) and we may represent a given model by $\mathbf{m}$, a vector of dimension $3N$. We further limit M by requiring that it encompass only physically realizable models. A model is said to be physically realizable if each shell's properties satisfy

$$\rho > 0, \tag{54a}$$

$$\mu \geq 0, \tag{54b}$$

and

$$\lambda \geq -\frac{2}{3}\mu, \tag{54c}$$

where both equalities 54b and 54c are not simultaneously true. The latter two constraints merely express the condition that an elastic material be thermodynamically stable (Fung, 1965).

Let ${}_n\omega_l(\mathbf{m})$ be the n^{th} overtone of the spheroidal mode of degree l associated with the model $\mathbf{m}$. (Both n and l range over the non-negative integers.) We cannot express ${}_n\omega_l(\mathbf{m})$ in closed analytic form but we can, through techniques previously discussed, generate it numerically. We can now formulate the inverse problem in the following manner.

Let ${}_n\omega_{li}^0$, $i = 1, \ldots, K$ be observed resonant frequencies associated with particular modes of oscillation. We wish to determine a model $\mathbf{m}$, satisfying

$${}_{ni}\omega_{li}(\mathbf{m}) = {}_{ni}\omega_{li}^0 \qquad i = 1, \ldots, K. \tag{55}$$

As Backus and Gilbert (1967) have pointed out, we do not know, *a priori*, if the set of solutions to eq 55 is empty, has a single member, or is a subspace of M of one or more dimensions.

We do not know a direct procedure for solving eq 55 for one or more models $\mathbf{m}$. We resort here to iterative methods for, hopefully, generating successively improved approximations for $\mathbf{m}$. For convenience we rewrite eq 55 as

$$D_i(\mathbf{m}) = D_i^0 \qquad i = 1, \ldots, K \tag{56}$$

where the D_i^0 are *data* and the $D_i(\mathbf{m})$ are *data functions*. $D_i(\mathbf{m})$ is a scalar-valued function whose domain is the $3N$-dimensional vector space M and whose value is the angular frequency of free oscillation of the n_i^{th} overtone of degree l_i. Let $\mathbf{m}_0$ be some model which we believe to lie near $\mathbf{m}$. We wish to find some perturbation, $\delta\mathbf{m}$, in $\mathbf{m}^0$, such that $\mathbf{m}^0 + \delta\mathbf{m}$ more nearly satisfies eq 56. ($\mathbf{m}^0$ and $\mathbf{m}^0 + \delta\mathbf{m}$ must both lie in M but $\delta\mathbf{m}$ alone need not.) We wish to have

$$D_i(m^0 + \delta m) = D_i^0 \qquad i = 1, \ldots K. \tag{57}$$

Expanding $D_i(\mathbf{m})$ in a Taylor series gives

$$D_i(\mathbf{m}^0 + \delta\mathbf{m}) = D_i(\mathbf{m}^0) + \sum_{j=1}^{3N} \left[\frac{\partial D_i}{\partial m_j}\right]_{\mathbf{m}^0} \delta m_j + O(|\delta\mathbf{m}|^2) \qquad i = 1, \ldots K. \tag{58}$$

Then, to first order in $|\delta\mathbf{m}|$, we wish $\delta\mathbf{m}$ to satisfy

$$\sum_{j=1}^{3N} \left[\frac{\partial D_i}{\partial m_j}\right]_{\mathbf{m}^0} \delta m_j = D_i^0 - D_i(\mathbf{m}^0) \qquad i = 1, \ldots K. \tag{59}$$

If $|\delta\mathbf{m}|$ is sufficiently small we may expect that $\mathbf{m}^1 = \mathbf{m}^0 + \delta\mathbf{m}$ will more nearly satisfy eq 56 than $\mathbf{m}^0$ did. As a measure of a model's suitability , we may define

$$\epsilon(\mathbf{m}) = \sum_{i=1}^{K} \frac{|D_i(\mathbf{m}) - D_i^0|}{D_i^0}. \tag{60}$$

Equations 59 constitute a $K \times 3N$ set of linear equations in the components of $\delta\mathbf{m}$. We may not, in general, expect to find $\delta\mathbf{m}$ exactly satisfying eq 59 for all possible cases. If the rank of the system does not exceed $3N$, such a $\delta\mathbf{m}$ exists but is not necessarily unique. If the rank exceeds $3N$, it does not exist.

Various methods of solution have been applied to the system 59 (Backus and Gilbert, 1967; Anderson and Smith, 1968; Smith and Franklin, 1969; Jordan and Franklin, manuscript, 1971). We adopt here a general technique proposed by Franklin, (unpublished manuscript, 1969.)

We rewrite eq 59 more compactly as

$$\underline{A}(\mathbf{m}^0) \cdot \delta\mathbf{m} = \mathbf{R}(\mathbf{m}^0) \tag{61}$$

where $\underline{A}(\mathbf{m}^0)$ is the matrix whose elements a_{ij} are

$$a_{ij}(\mathbf{m}) = \left[\frac{\partial D_i}{\partial m_j}\right]_{\mathbf{m}} \tag{62}$$

and $\mathbf{R}(\mathbf{m}^0)$ is the vector of data residuals whose i^{th} component is $D_i^0 - D_i(\mathbf{m}^0)$. We now regard eq 61 as a linear relation between three stochastic processes: a signal process, a data process and a noise process. $\delta\mathbf{m}$ is a sample of the signal process, and $\mathbf{R}(\mathbf{m}^0)$ is the sum of a sample of the data process plus a sample of the noise process. Each process is taken to have zero expectation.

The use of stochastic techniques to solve eq 61 is based, in part, upon contemplation of some of the potential sources of error entering into the relation. The measured spectral values D_i^0 are contaminated by measurement error and possible mode misidentification. The physical system upon which measurements are made may deviate from the class of models M in which $\mathbf{m}$ must lie. It is possible that there is no model $\mathbf{m}$ in M that would then satisfy eq 56.

Let $\mathbf{R}^m$ denote the autocorrelation associated with the signal process $\delta\mathbf{m}$, and $\underline{R}^0$ denote the autocorrelation operator associated with the noise process. $\underline{R}^m$ is a $3N \times 3N$ square matrix whose $(i, j)^{th}$ component is the expectation of the product $\delta m_i \delta m_j$. $\underline{R}^0$ is defined analogously. The best linear estimate for $\delta\mathbf{m}$ is given by (Franklin, 1969):

$$\delta\mathbf{m} = \underline{R}^0 \cdot \underline{A}(\mathbf{m}^0) \cdot [\underline{A}(\mathbf{m}^0) \cdot \underline{R}^m \cdot \underline{A}^T(\mathbf{m}^0) + \underline{R}^0]^{-1} \cdot \mathbf{R}(\mathbf{m}^0). \tag{63}$$

A solution, $\delta\mathbf{m}$, can be guaranteed to exist if $\underline{R}^0$ is a positive definite matrix.

Pending the acquisition of experience, we will forego at this time any suggestions about the fabrication of $\underline{R}^m$ and $\underline{R}^0$.

We have outlined above a method for inverting measured eigenvalue spectra to produce a model $\mathbf{m}$ consistent with the spectra. The only remaining theoretical problem is the computation of the partial derivatives,

$$\left[\frac{\partial D_i}{\partial m_j}\right]_{\mathbf{m}^0},$$

which form the components of $\underline{A}(\mathbf{m}^0)$. These expressions are, typically, extracted by applying Rayleigh's principle. Particularly good discussions are available in Backus and Gilbert (1967) and Dahlen (1968). We give here only the results. If λ, μ and ρ in a particular layer are altered by small amounts, the resulting alteration in ω is given by

$$\delta\omega = \frac{\left\{\int_0^{r_N} (\delta\lambda\Lambda + \delta\mu M \quad \delta\rho R) r^2 dr\right\}}{\left\{2\omega \int_0^{r_N} [U^2 + l(l+1)V^2]\rho r^2 dr\right\}} \tag{64}$$

where

$$\Lambda = (\partial_r U + r^{-1}F)^2, \tag{65a}$$

$$M = 2(\partial_r U)^2 + l(l+1)r^{-2}[U + (r\partial_r - 1)V]^2 +$$

$$+ r^{-2}F^2 + r^{-2}(l-1)l(l+1)(l+2)U^2, \tag{65b}$$

$$R = -\omega^2[U^2 + l(l+1)V^2], \tag{65c}$$

and

$$F = 2U - l(l+1)V. \tag{65d}$$

Preliminary Experimental Results

As a first step in the validation of the foregoing theoretical results we elected to attempt to measure the normal mode spectra of layered spheres of known composition. Spherical samples are, in general, difficult to prepare, and our first specimen was composed of a thin steel shell filled with distilled water.

The steel shell was formed by joining two stainless steel hemispheres with epoxy. The sphericity and homogeneity of the resulting shell is open to question; the hemispheres were procured from an industrial float works. However, we believed that mechanical perfection was not, at this point, necessary.

A small transducer was bonded to the shell and the sample was placed in the experimental arrangement shown in Figure 12. Coupling between the sample and the "driving" transducer was weakened by inserting rubber padding and an "O" ring between the two. Some experimentation indicated that coupling in this configuration is sufficiently weak that the measured spectra are not significantly influenced.

The apparatus produced a graphical record of the response of the sample to a sinusoidal source as a function of frequency. A portion of that result is recorded in Figure 13. The center frequency of significant peaks is given above each such peak. The amplitude scale is arbitrary, but linear. Tentative assignments of peaks to a particular mode are indicated by the designation ${}_nS_l$, where n is the overtone number and l is the harmonic degree.

Figure 14 is a juxtaposition of the observed resonance frequencies and the values computed for a sphere composed of an inner core of density 0.998, having a compressional velocity of 1.498×10^5, and a radius of 7.62. The core is surrounded by a shell of thickness 0.0904, with a density of 7.3772 and having compressional and shear velocities of, respectively, 5.79×10^5 and 3.1×10^5. We regard the agreement as being generally satisfactory.

In Figure 13, it can be seen that we have, in several instances, assigned a mode to a small collection of adjacent peaks. Perturbation theory (Dahlen, 1968) tells us that small deviations from spherical symmetry will generally split the $2l + 1$ individual modes associated with a given (n, l) pair apart in frequency. That is, asphericities either remove, or at least decrease, the degeneracy of a particular mode. (Only the family ${}_nS_0$ is not degenerate, and it, too, can still be shifted.) It is not unreasonable to expect that the abundant asphericities present in our sample will produce such an effect and that, for instance, the twin peaks associated with ${}_oS_2$ in Figure 13 are an expression of this. We believe that such effects can be greatly reduced by increasing the mechanical symmetry of the sample.

The sample fabrication method used above is not a particularly happy one for routine measurements of the properties of fluids. Figure 15 shows the partial derivative of eigenfrequency with

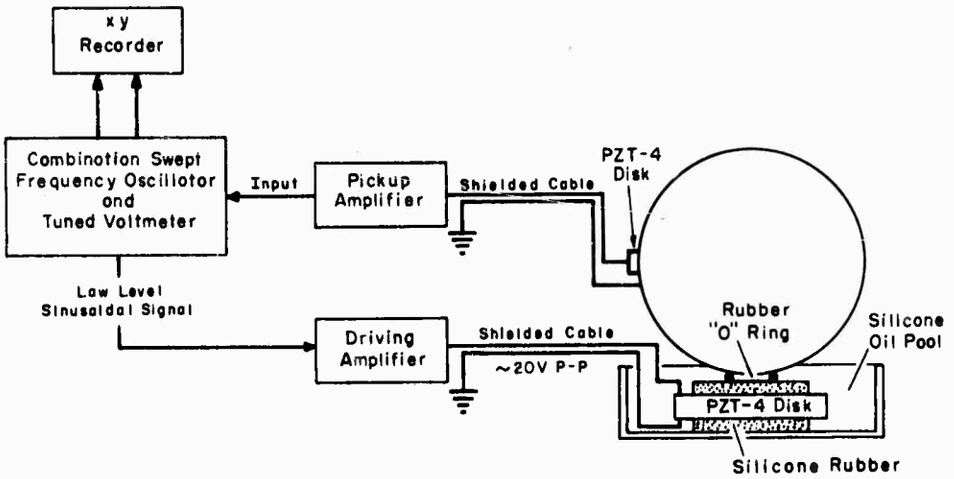

Figure 12. Experimental apparatus used to measure frequencies of free oscillation.

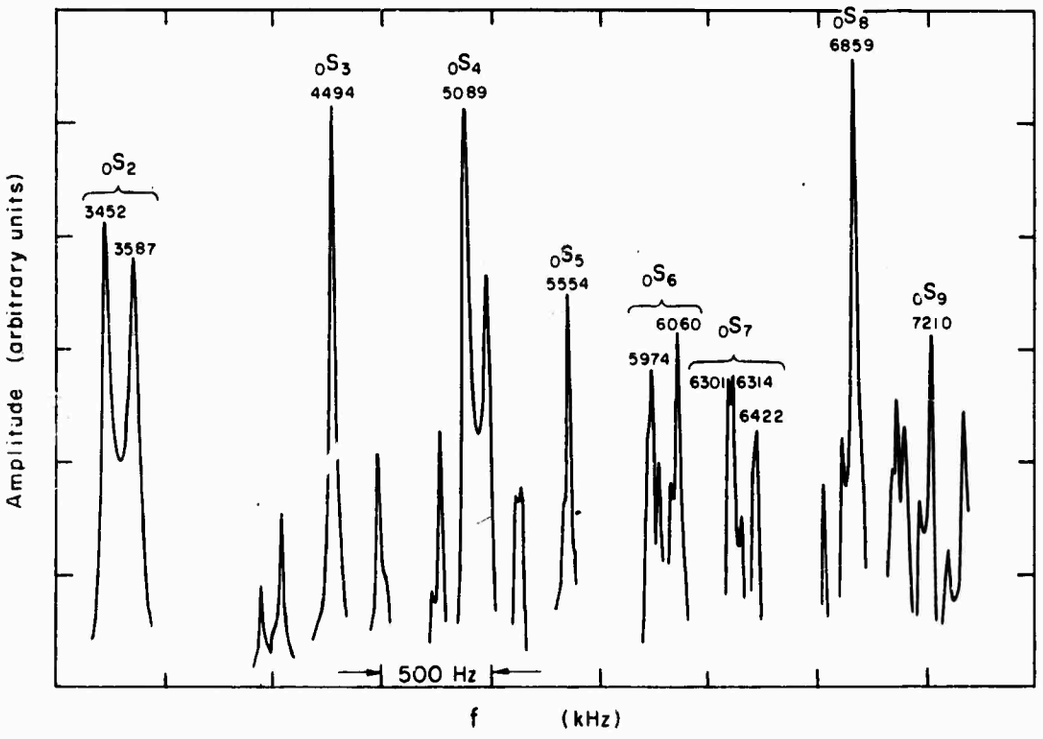

Figure 13. Portion of the measured spectrum of a stainless steel shell 0.040 in. thick and 6 in. O.D., filled with distilled water. Peak frequencies are shown and tentative mode assignments, based on handbook data, are indicated.

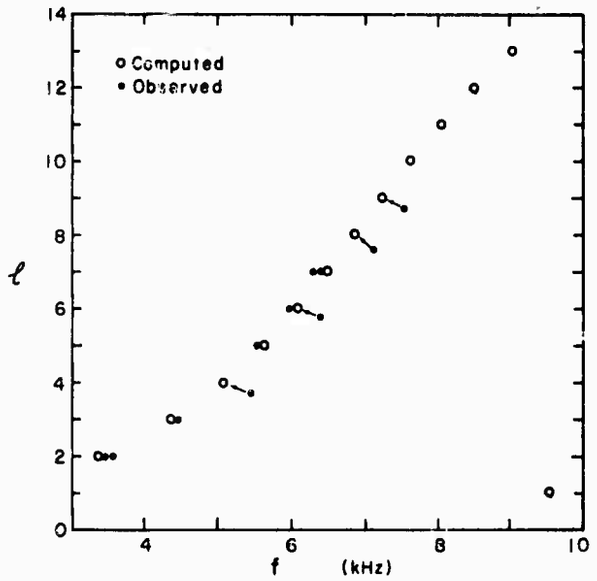

Figure 14. Open circles represent loci, in the (f, l) plane, of the frequencies of free oscillation, computed for a stainless steel shell, filled with distilled water, of the dimensions used in the experiment. Filled circles indicate measured resonances. Arrows indicate overlapping symbols. Assignment of an ordinate to measured frequencies is arbitrary.

respect to compressional velocity in the fluid and the shell, and shear velocity in the shell, as a function of l, for the fundamental modes ${}_0S_l$. We see that for $l \geq 2$ shear velocity in the shell dominates all other controlling parameters, and that for $l \geq 5$ compressional velocity in the fluid is the least significant parameter. At $l = 13$, compressional velocity in the fluid is about 1/40 as important as shear velocity in the shell.

A preferable arrangement is one in which the quantity of interest is the controlling parameter. One way to achieve this is to utilize higher-order overtones. For example, for ${}_1S_3$ we have

$$\frac{\partial f}{\partial V_p} = 0.126 \qquad \text{(fluid core)},$$

$$\frac{\partial f}{\partial V_p} = 1.65 \times 10^{-6} \qquad \text{(shell), and}$$

$$\frac{\partial f}{\partial V_s} = 3.39 \times 10^{-3} \qquad \text{(shell)}.$$

Thus ${}_1S_2$ is substantially more influenced by the properties of the fluid than by those of the shell. This behavior results, in a general way, from the increasing concentration of energy in the interior associated with higher and higher overtones. Unfortunately one result of this is that such modes are difficult to excite, or observe, from the surface.

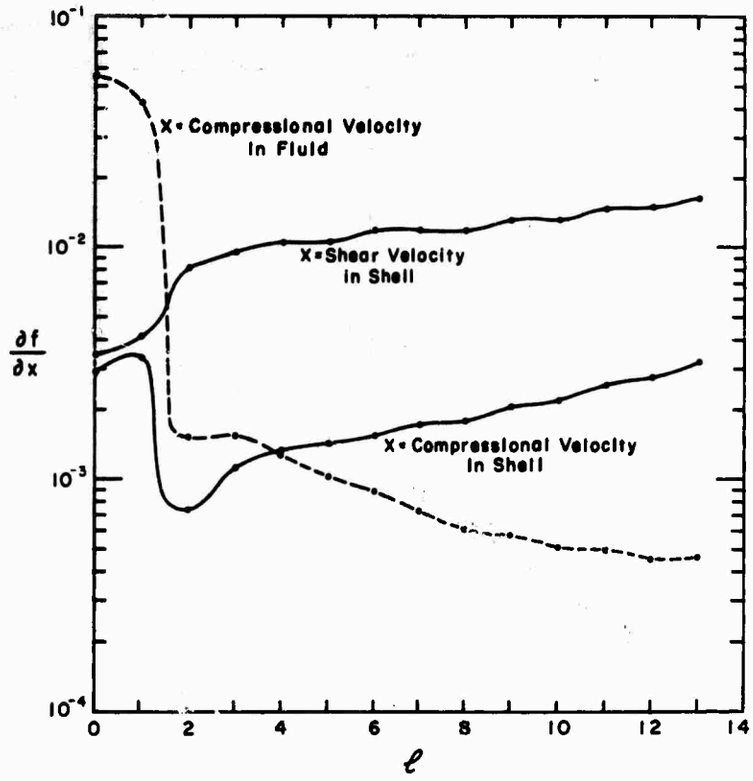

Figure 15. The partial derivatives of the fundamental frequencies of free oscillation, as a function of l and with respect to various indicated properties, of a water-filled steel shell. For visual ease, the derivatives have been joined by smooth curves.

A more promising approach is to use shells composed of a material, such as Lucite, whose properties do not represent as severe an impedance contrast to the interior material. Exploratory calculations are presently being made on the optimum shell composition. We are also arranging to have shells machined, as opposed to other methods of fabrication, to greatly reduce the variations and asphericities of the sample.

The preparation of spherical soil samples proved to be considerably more difficult, owing to the volume change of water upon freezing. After extensive experimentation we were finally able to form a frozen soil inside a spherical steel shell by maintaining strong temperature gradients across the sample while allowing for the venting of unfrozen water from the sphere.

Figure 16 shows a portion of the resonance spectrum for a 4-in.-diameter sphere of frozen, fully saturated 20/30 Ottawa banding sand. The experimental arrangement used in this measurement differed from that depicted in Figure 12 in that a) the sphere was supported on inflated plastic cushions and b) the applied signal consisted of a four cycle tone burst generated every 10 milliseconds.

The modes ${}_0S_2$ and ${}_0S_0$, together with their partial derivatives, were used to estimate the compressional and shear velocities of the frozen soil. Forward calculations for the new model are shown in Table IV and compared to the data. The maximum relative error for the lowest five observed modes is 3.7% for ${}_0S_3$, which Figure 16 shows as being badly split.

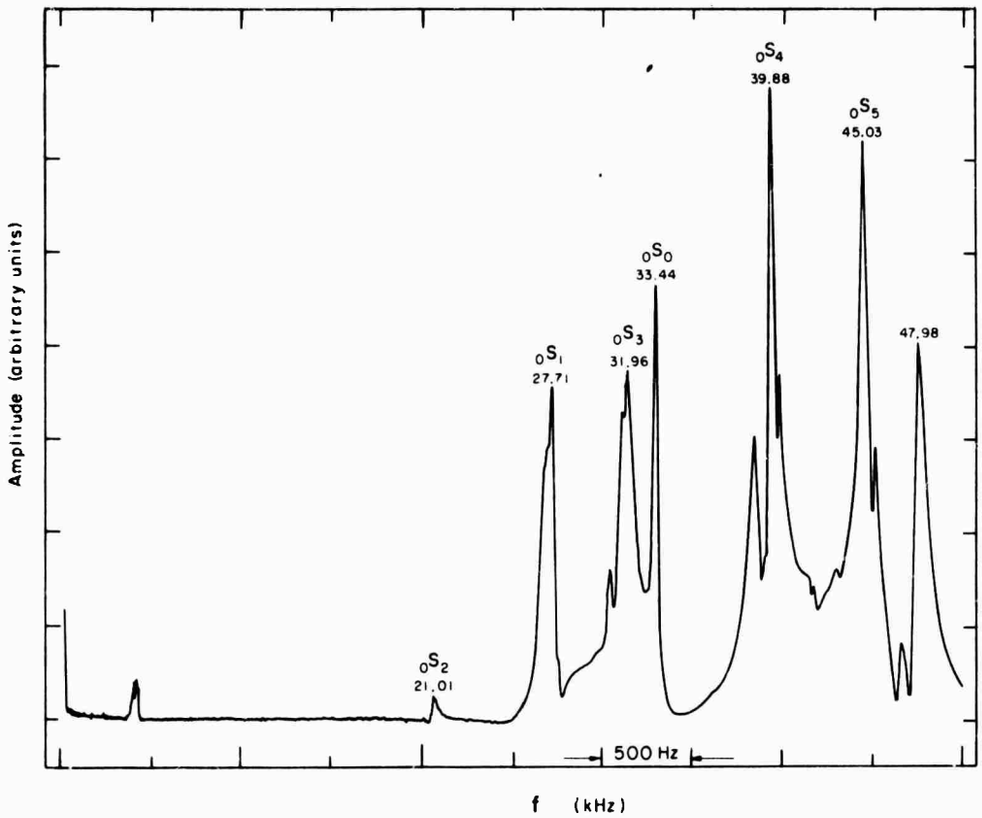

Figure 16. Portion of the measured spectrum of a stainless steel shell, 0.040 in. thick and 4 in. O.D. filled with frozen, saturated, 20/30 Ottawa banding sand at –38°C.

Table IV. Computed and observed frequencies of free oscillation of a saturated, frozen 20/30 Ottawa banding sand sample encased in a steel shell.

Mode	Computed[1] (kHz)	Observed (kHz)	Comp-Obs / Comp
oS_2	21.01	21.01	0
oS_1	27.72	28.11	-1.4×10^{-2}
oS_3	30.96	31.96	-3.2×10^{-2}
oS_0	33.42	33.44	-6×10^{-4}
oS_4	39.38	39.88	-1.3×10^{-3}
oS_5	47.14	?2	

1. Computed for $r_1 = 4.961$ cm, $V_{p1} = 4.391 \times 10^5$ cm/sec, $V_{s1} = 2.66 \times 10^5$ cm/sec, $\rho_1 = 2.0$, $r_2 = 5.062$ cm, $V_{p2} = 5.79 \times 10^5$ cm/sec, $V_{s2} = 3.1 \times 10^5$ cm/sec, $\rho_2 = 7.8772$.

2. Splitting for oS_5 is too severe to allow a useful result.

Conclusions and Projected Research

We believe that this procedure will provide a theoretically straightforward and experimentally practical method of measuring the elastic properties of solids and fluids, and in particular, of frozen ground. We further expect, with the existing apparatus, to be able to measure Q, or attenuation, simultaneously with the elastic properties. (The necessary theory for attenuation measurements is well-developed. See Anderson and Archambeau (1964).)

The technique should be particularly useful in discerning small variations of elastic properties as a function of temperature. Such information is of value in deciphering the physical chemistry of frozen soils through, and near, the freezing point.

Literature Cited

Anderson, D.L. and C.B. Archambeau (1964) The anelasticity of the earth. *Journal of Geophysical Research*, vol. 69, p. 2071-2084.

Anderson, D.L. and M.L. Smith (1968) Mathematical and physical inversion of gross earth data. Paper presented at Am. Geophys. Union Annual Meeting, Washington, D.C.

Backus, G.E. (1967) Converting vector and tensor equations to scalar equations in spherical coordinates. *Journal of Geophysical Research of the American Society*, vol. 13, p. 71-101.

Backus, G.E. and J.F. Gilbert (1967) Numerical applications of a formation for geophysical inverse problems. *Journal of Geophysical Research of the American Society*, vol. 13, p. 247-276.

Bullen, K.E. (1963) *Introduction to the theory of seismology*. London: Cambridge University Press.

Dahlen, F.A. (1963) The normal modes of a rotating elliptical earth. *Journal of Geophysical Research of the American Society*, vol. 16, p. 329-367.

Fung, Y.C. (1965) *Foundations of solid mechanics*. New Jersey: Prentice Hall.

Hildebrand, F.B. (1956) *Introduction to numerical analysis*. New York: McGraw-Hill.

Hill, E.L. (1954) The theory of vector spherical harmonics. *American Journal of Physics*, vol. 22, p. 211-214.

Love, A.E.H. (194) A treatise on the mathematical theory of elasticity. Dover, New York.

Smith, M.L. and J.N. Franklin (1969) Geophysical applications of generalized inverse theory. *Journal of Geophysical Research*, vol. 74, p. 2783-2785.

Sternberg, E. (1960) On the integration of the equations of motion in the classical theory of elasticity. *Arch. for Rat. Mech. and Anal.*, vol. 6, p. 34-50.

BLANK PAGE

IV. DETERMINATION OF ACOUSTIC PROPERTIES OF FROZEN EARTH MATERIALS BY THE USE OF A CRITICAL ANGLE TANK

by

Y. Nakano, M. Smith and R. Martin

Introduction

One of the standard methods for determining acoustic properties of earth materials is an ultrasonic technique using a critical angle tank. In spite of its inherent interpretive problems, it theoretically allows simultaneous operation in both dilatation and shear at wavelengths small compared to the sample thickness.

The method, applied to metal, was first described by Schneider and Burton (1949) and subsequently used by Subbarao and Rao (1957) on rocks. King and Fatt (1962) used it to determine velocities in rock specimens subjected to confining pressures, and Wyllie et al. (1962), Gregory (1963), and Banthia et al. (1965) applied the techniques to determine velocities in rocks under both differential external confining pressures and internal pore fluid pressures. Recently Attewell (1970) used this method to study triaxial anisotropy of rocks.

In the present work dilatational and shear wave velocities, as well as attenuation of several standard frozen soils, were determined by the use of the critical angle tank.

Experimental Apparatus

The critical angle tank is constructed from ½-inch-thick Plexiglas, 13 inches long × 9 inches wide × 9 inches deep (Fig. 17). At either end, a transducer mounted on an aluminum rod is inserted through the wall of the tank by means of an O-ring seal. The distance between the two transducers can be changed. One transducer, made of 2.5-inch-diameter × 0.5-inch-thick PZT4, serves as a transmitter for producing uniform plane dilatational waves. The transmitter is connected to a Wayne Kerr Model SR-268 signal generator via a General Radio Model 1396-B tone-burst generator so that a harmonic burst of any number of cycles can be sent to the transmitter with any desired time interval. The other transducer, of 1.0-inch- diameter × 0.5-inch-thick PZT4, serves as a receiver, and is connected to a Tektronix type 567 dual-trace oscilloscope via a Krohn-hite filter, which passes only signals of a specified frequency range. One trace of the oscilloscope is triggered directly from the pulse generator to display received signals. The other oscilloscope trace is used for a Rutherford Electronics time delay generator, which is triggered by the pulse generator and is used for accurate measurements of arrival time with error less than ±0.1 sec.

The tank is filled with Dow Corning 200 silicone oil used both as a cooling medium and as a medium for transmitting the input pulses across the tank to the receiver. The cooling medium is

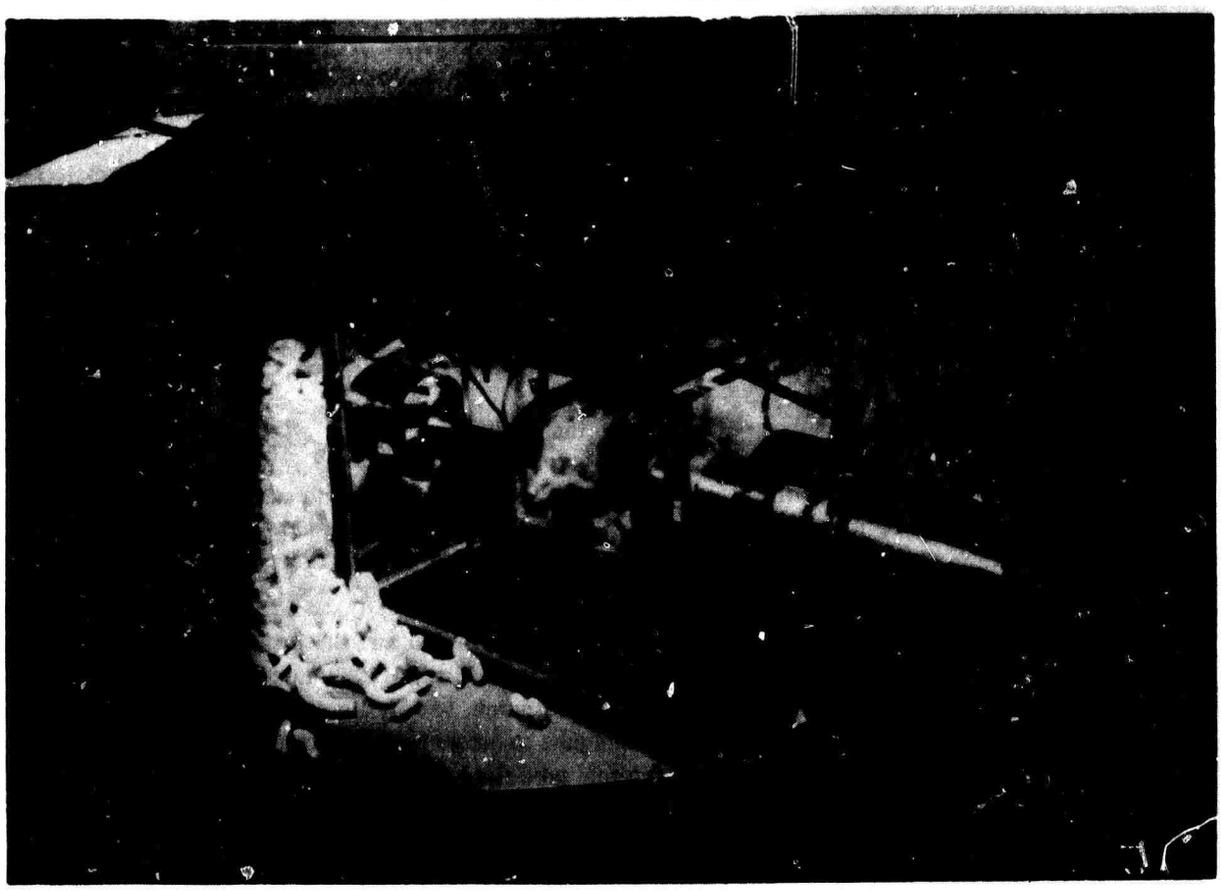

Figure 17. Critical angle tank.

circulated through a Forma Scientific Model 2095 refrigerated bath which maintains the required temperature. A sample holder 7 inches long × 8 inches deep that can hold a specimen up to 1 inch thick is placed vertically inside the tank. A frozen soil specimen, 4.5 inches in diameter, is mounted at the center of the sample holder so as to intercept the ultrasonic beam. The surface of the frozen soil specimen is sealed by a thin vinyl sheet. The sample can be rotated about a vertical axis running through the center of the tank, the angle of rotation of the sample from normal beam incidence being indicated on a circular dial graduated in degrees and readable to 0.1° by means of a vernier scale.

Theory

A transmitted sound wave, after passing through the fluid, strikes the sample at an angle i to its normal (Fig. 18a). Of the incident dilatational energy, part is reflected back at an angle i and part is transmitted into the sample. Since the dilatational velocity C_p in frozen soils (~ 4.0 km/sec) greatly exceeds that (C_w) in silicone oil (~ 1.0 km/sec), the transmitted (refracted) portion of the incident energy is rotated from the normal at an angle $\theta_p > i$ according to Snell's law:

$$\theta_p = \sin^{-1}\left(\frac{C_p}{C_w}\sin i\right). \qquad (1)$$

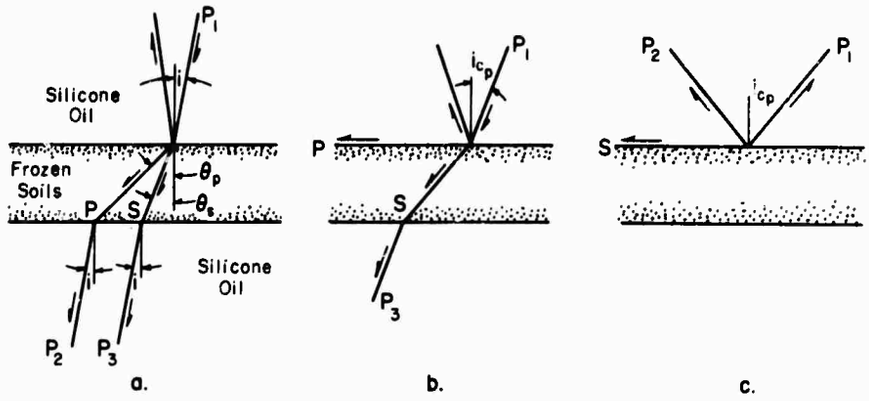

Figure 18. Reflection and refraction geometry of a beam of dilatational pulses on a slab of frozen soils in silicone oil. (a) Near normal incidence. (b) Critical refraction of the dilatational beam. (c) Critical refraction of the shear beam.

The component of the particle motion not accounted for by the transmitted dilatation P forms a shear wave S which is refracted at a small angle θ_s ($<\theta_p$) since $C_p > C_s$ (~ 2.0 km/sec) $> C_w$. S is polarized within the plane of incidence again according to Snell's law:

$$\theta_s = \sin^{-1}\left(\frac{C_s}{C_w}\sin i\right). \tag{2}$$

At the second surface of the sample, since fluid cannot accommodate the shear mode, both wavetrains are refracted back towards the normal at an angle i in the form of dilatational waves and activate the receiving transducer. Each of the shear and dilatational signals striking the second surface will, in general, give rise to both shear and dilatational waves, in the sample, which emanate from the interface. However, by considering only the first portion of the received signal we may eliminate these.

As i is increased by mechanical rotation of the sample, a critical angle i_{cp} is reached (Fig. 18b) at which P skims across the surface of the sample in a transitional stage between refraction and reflection. At this stage, from eq 1,

$$C_p = \frac{C_w}{\sin(i_{cp})}. \tag{3}$$

As i is increased still further, P becomes totally reflected and at a second critical angle, i_{cs} ($> i_{cp}$), S skims across the surface of the sample (Fig. 18c). (In fact, reflection is complete only if the sample is infinite in thickness. Signals incident at, or beyond, the critical angle will "tunnel" through a finite sample in a fashion exactly analogous to the well-known quantum mechanical phenomenon. For samples greater than a few wavelengths, we may disregard this effect.) Again, from eq 2,

$$C_s = \frac{C_w}{\sin(i_{cs})}. \tag{4}$$

At normal incidence the beam travels the shortest dimension of the sample and suffers minimal attenuation. As i is increased, the wave path in the sample increases and the transmitted pulse amplitude decreases. When $i = i_{cp}$, P is removed from the transmitted beam and the resolved amplitude for i_{cp} exhibits, in practice, an intermediate minimum rather than an inflection on the curve. At $i = i_{cs}$, S is eliminated from transmission and one is left with an absolute minimum amplitude. In practice, the theoretical sequence of events outlined above is disorganized as a result of the interference between the incident beam and reflected beams within the specimen. Interference patterns often lead to difficulty in locating i_{cp} with precision. Therefore, another method, a fluid displacement technique, was used to determine dilatational velocities in the present work. The difference in delay time δt between the pulses received after crossing the liquid path alone as compared with their passage through liquid and specimen interposed at normal incidence produces a value for C_p in the following way. If t_1 is the time delay arising from transmission across the tank through liquid alone and l_w is the wave path in liquid, then $t_1 = l_w/C_w$. The time delay arising from transmission across the tank when a sample is interposed at normal incidence is,

$$t_2 = \frac{l_w - d}{C_w} + \frac{d}{C_p}$$

where d is the sample thickness. Then the difference in both delays is,

$$t = t_1 - t_2$$

$$= d\left(\frac{1}{C_w} - \frac{1}{C_p}\right).$$

Therefore,

$$C_p = \frac{C_w d}{d - C_w \delta t}. \tag{6}$$

The attenuation is determined from the measurement of the ratio of the amplitudes A_i and A_j of the received waves for specimens of two different thicknesses L_i and L_j, respectively (Auberger and Rinehart, 1961). Namely, the attenuation coefficient α (nepers/cm) is given as:

$$\alpha = \frac{\ln (A_i/A_j)}{(L_j - L_i)}$$

or the value of Q is given as:

$$Q = \frac{(\pi/\lambda)(L_j - L_i)}{\ln (A_i/A_j)}$$

where λ is a wavelength.

Results and Discussion

We examined three standard types of soils, Ottawa sand, Hanover silt, and Goodrich clay, whose gradation curves obtained according to ASTM test procedures are shown in Fig. 1. The size of the specimen used for velocity measurements is 4.5 inches in diameter × 1.0 inch thick. All measurements were made at subzero temperature due to the fragility of the sample holding device.

Dilatational wave velocity

Velocity of dilatational waves was measured as a function of temperature and frequency. It was found that the frequency has no distinguishable effect on dilatational velocities in the range between 300 kHz and 1.2 MHz examined. Fig. 19 shows the observed dilatational velocities as a function of temperature. The detailed discussion on the correlation between the dilatational velocity and temperature or unfrozen water content is presented in another part of this report.

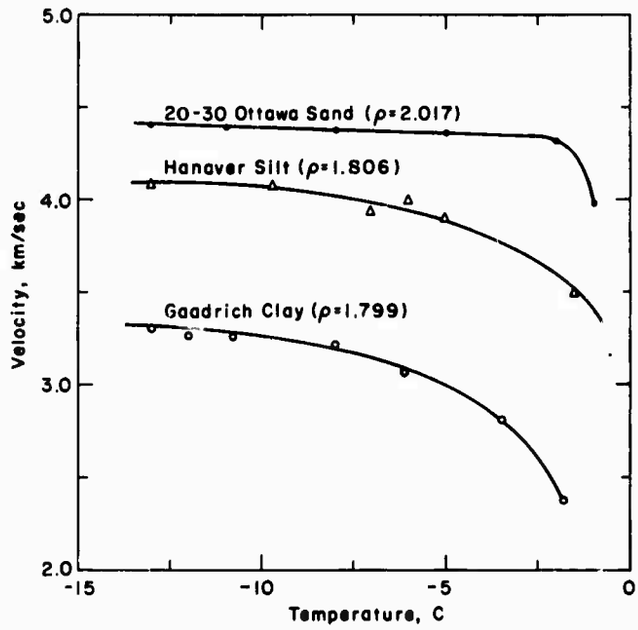

Figure 19. Dilatational velocity vs temperature.

Shear wave velocity

Measured shear velocities are shown in Figure 20 as a function of temperature. Although the data are somewhat scattered, there is a general tendency for the shear velocity to decrease with ascending temperature. The roll of unfrozen water in shear wave propagation is more complicated than the decrease of velocity as in dilatational wave propagation. Since liquid water cannot accommodate the shear mode, shear waves are expected to attenuate severely while traveling through a layer of liquid water. Therefore the crystalline matrices consisting of soil minerals and possibly ice are the path through which shear waves propagate. In view of the fact that the slope of velocity-temperature curves does not differ markedly among the tested samples, soil mineral matrix might play a major roll. Since the soil samples used are well packed, soil minerals must contact each other

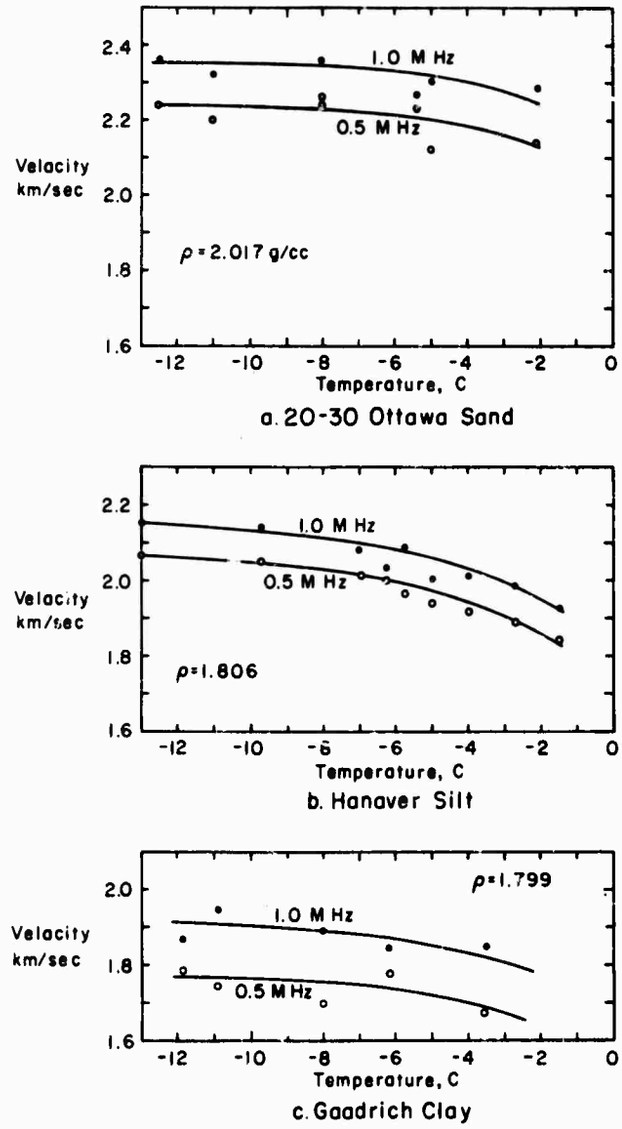

Figure 20. Shear velocity vs temperature for 20-30 Ottawa sand, Hanover silt, and Goodrich clay.

closely. If the soil is not well packed, a different result might be obtained. The shear velocities of crystalline rock and polycrystalline ice are about 3.0 km/sec and 1.6 km/sec respectively. The measured shear velocities of frozen soils fall between these two bounds.

The shear velocity was found sensitive to frequency in an almost linear manner in the range of 0.3 MHz to 1.2 MHz. The velocity increases with increasing frequency. This trend was also reported by Attewell (1970), who measured the shear velocity of the Penrhyn slate of North Wales using the critical angle method. He claimed that the shear wave dispersion resulting in frequency dependence of velocity is a function of the critical angle technique and does not represent the shear velocity conditions in the slate. Any increase of velocity with frequency implies distortion of the spectrum of traversing waves through the solid. Although Attewell's reasoning based upon much

experimental evidence is convincing, the reason why the critical angle technique does not accurately represent the shear conditions in the slate was not explained.

Since we do not have sufficient experimental results, we are not able to evaluate the accuracy of shear velocity measurements in frozen soils. Further efforts are needed to clarify this problem.

Attenuation of dilatational waves

Attenuation of waves in earth materials at high frequency is one of the least understood phenomena. Wyllie et al. (1962) stated that attempts to measure attenuation in porous media at frequencies higher than 100 kHz gave equivocal results. Auberger and Rinehart (1961) measured attenuation of longitudinal waves in rocks by the pulse method in the frequency range 0.2 MHz to 1.0 MHz. No definite conclusion was made on the correlation between frequency and attenuation, since attenuation does not follow any marked law of increase or decrease with frequency. Attewell (1970) reported attenuation of dilatational waves in hard blue Penrhyn slate by the critical angle technique in the frequency range 0.5 MHz to 5.0 MHz. He did not describe any difficulty or problem concerning attenuation measurement.

We measured the attenuation of dilatational waves in frozen soils by using samples of different thickness. Although the wave patterns of the received signals for samples of different thickness resemble each other and the amplitude of an initial rise or first arrival can be measured without difficulty, we are plagued by lack of reproducibility. We do not know whether this is inherent in the frozen soils examined or is due to error in measurements. Therefore we are not able to present our results in this report.

Literature Cited

Attewell, P.B. (1970) Triaxial anisotropy of wave velocity and elastic moduli in slate and their axial concordance with fabric and tectonic symmetry. *Int. J. Rock Mech. Min. Sci.*, vol. 7. p. 193-207.

Banthia, B.S.; M.S. King and I. Fatt (1965) Ultrasonic shear wave velocities in rocks subjected to simulated overburden pressure and internal pore pressure. *Geophysics*, vol. 20, p. 117-121.

Gregory, A.R. (1963) Shear wave velocity measurements of sedimentary rock samples under compression. *Proceedings of the 5th International Symposium on Rock Mechanics*, University of Minnesota (C. Fairhurst, Ed.), p. 439-471.

King, M.S. and I. Fatt (1962) Ultrasonic shear wave velocities in rocks subjected to simulated overburden pressure. *Geophysics*, vol. 27, p. 590-598.

Schneider, W.C. and C.J. Burton (1949) Determination of the elastic constants of solids by ultrasonic methods. *J. Appl. Phys.*, vol. 20, p. 48-58.

Subbarao, K. and B.R. Rao (1957) A simple method of determining ultrasonic velocities in rocks. *Nature*, Lond., vol. 180, p. 978.

Wyllie, M.R.J.; G.H.F. Gardner and A.R. Gregory (1962) Studies of elastic wave attenuation in porous media. *Geophysics*, vol. 27, p. 569-589.

Auberger, M. and J.S. Rinehart (1961) Ultrasonic velocity and attenuation of longitudinal waves in rocks. *JGR*, vol. 66, p. 191-199.

BLANK PAGE

APPENDIX A. ANALYTIC SOLUTIONS OF THE TRANSFORMED WAVE EQUATION

We represent **u** by

$$\mathbf{u} = \nabla\psi + \nabla \times \vec{r}r\chi + \nabla \times \nabla \times \vec{r}r\sigma \tag{A1}$$

where ψ, χ and σ are scalar fields. The representation A1 was chosen because it is "natural" to the field equations (eq 3).

It is helpful to develop the following useful expressions

$$\nabla \cdot \mathbf{u} = \nabla^2\psi,$$

and

$$\nabla \times \nabla \times \mathbf{u} = \nabla \times \nabla \times \nabla \times (\vec{r}r\chi) + \nabla \times \nabla \times \nabla \times \nabla \times (\vec{r}r\sigma) =$$

$$= \nabla \times \{\nabla(\nabla \cdot \vec{r}r\chi) - \nabla^2(\vec{r}r\chi)\} +$$

$$+ \nabla \times \nabla \times \{\nabla(\nabla \cdot \vec{r}r\sigma) - \nabla^2(\vec{r}r\sigma)\}.$$

We expand $\nabla^2(\vec{r}r\chi)$ as

$$\nabla^2(\vec{r}r\chi) = \vec{r}\left\{\nabla^2(r\chi) - \frac{2}{r}\chi\right\} + \nabla_1\left\{\frac{2}{r}\chi\right\}$$

$$= \vec{r}r\,\nabla^2\chi + \nabla\{2\chi\}$$

as may easily be shown by expanding. So,

$$\nabla \times \nabla \times u = -\nabla \times \vec{r}r\,\nabla^2\chi - \nabla \times \nabla \times \vec{r}r\,\nabla^2\sigma.$$

If we insert these into the field equation (eq 3) and regroup terms, we find

$$\nabla\{\rho\partial_t^2\psi - (\lambda + 2\mu)\nabla^2\psi\} + \nabla \times \vec{r}r\{\rho\partial_t^2\chi - \mu\nabla^2\chi\} +$$

$$+ \nabla \times \nabla \times \vec{r}r\{\rho\partial_t^2\sigma - \mu\nabla^2\sigma\} = 0.$$

In order to ensure that eq 3 is satisfied, it is sufficient that ψ, χ and σ be solutions to

$$\rho\partial_t^2\psi - (\lambda + 2\mu)\nabla^2\psi = 0, \tag{A2a}$$

$$\rho \partial_t^2 \chi - \mu \nabla^2 \chi = 0, \tag{A2b}$$

and

$$\rho \partial_t^2 \sigma - \mu \nabla^2 \sigma = 0. \tag{A2c}$$

We have not shown that all solutions to eq 3 can be expressed in terms of functions satisfying eq A2 and A1. These solutions are, however, known to be complete (Sternberg, 1960).

We now Fourier transform the system and introduce the expansions

$$\psi(r, \theta, \phi, \omega) = \sum_{l=0}^{\infty} \sum_{m=-l}^{l} \psi_l^m(r, \omega) Y_l^m(\theta, \phi), \tag{A3a}$$

$$\chi(r, \theta, \phi, \omega) = \sum_{l=1}^{\infty} \sum_{m=-l}^{l} \chi_l^m(r, \omega) Y_l^m(\theta, \phi), \tag{A3b}$$

and

$$\sigma(r, \theta, \phi, \omega) = \sum_{l=1}^{\infty} \sum_{m=-l}^{l} \sigma_l^m(r, \omega) Y_l^m(\theta, \phi). \tag{A3c}$$

The terms of degree $l = 0$ in the expansions for χ and σ have been omitted since they do not contribute to the displacement field, .

The expansions A3a-A3c are inserted into the transformed versions of A2a-A2c. We make use of eq 6 and 14 to simplify the result. If f is some scalar field, then by eq 6

$$\nabla f = \vec{r} \partial_r f + \nabla_1 (r^{-1} f)$$

and

$$\nabla^2 f = \partial_r^2 f + \frac{2}{r} \partial_r f + r^{-2} \nabla_1^2 f. \tag{A4}$$

The resulting expressions are multiplied by $\overline{Y_l^m(\theta, \phi)} \sin \theta$ and integrated over θ and ϕ. We appeal to the orthogonality relation 12. We then have

$$\left\{ \partial_r^2 + \frac{2}{r} \partial_r + \frac{\omega^2 \rho}{\lambda + 2\mu} - \frac{l(l+1)}{r^2} \right\} \psi_l^m(r, \omega) = 0, \tag{A5a}$$

$$\left\{ \partial_r^2 + \frac{2}{r} \partial_r + \frac{\omega^2 \rho}{\mu} - \frac{l(l+1)}{r^2} \right\} \chi_l^m(r, \omega) = 0, \tag{A5b}$$

and

$$\left\{\partial_r^2 + \frac{2}{r}\partial_r + \frac{\omega^2\rho}{\mu} - \frac{l(l+1)}{r^2}\right\}\sigma_l^m(r,\omega) = 0. \tag{A5c}$$

Each of the operators in brackets is some form of the spherical Bessel's operator. Its solutions are well-known and they are

$$\psi_l^m = A_l^m(\omega)\, j_l(kr) + B_l^m(\omega)\, y_l(kr), \tag{A6a}$$

$$\chi_l^m = C_l^m(\omega)\, j_l(\gamma r) + D_l^m(\omega)\, y_l(\gamma r), \tag{A6b}$$

and

$$\sigma_l^m = E_l^m(\omega)\, j_l(\gamma r) + F_l^m(\omega)\, y_l(\gamma r), \tag{A6c}$$

where

$$k = \frac{\omega}{\sqrt{\frac{\lambda + 2\mu}{\rho}}} \tag{A7}$$

and

$$\gamma = \frac{\omega}{\sqrt{\frac{\mu}{\rho}}}. \tag{A8}$$

We wish now to relate U, V and W to ψ, χ and σ. To do this, we will rearrange eq A1 to resemble eq 4. For convenience we will drop subscripts and superscripts.

We note immediately that

$$\nabla\psi = \vec{r}\partial_r\psi + \nabla_1(r^{-1}\psi).$$

Also,

$$\begin{aligned}\nabla \times \vec{r}r\chi &= r\chi\nabla \times \vec{r} - \vec{r} \times \nabla(r\chi)\\ &= -\vec{r} \times \nabla(r\chi)\\ &= -\vec{r} \times \nabla_1\chi.\end{aligned}$$

The third term can be expanded as

$$\begin{aligned}\nabla \times \nabla \times \vec{r}r\sigma &= \nabla(\nabla \cdot \vec{r}r\sigma) - \nabla^2(\vec{r}r\sigma)\\ &= -\vec{r}r\nabla^2\sigma - \nabla(2\sigma) + \nabla[r^{-2}\partial r(r^3\sigma)]\end{aligned}$$

$$\nabla \times \nabla \times \vec{r} r\sigma = \vec{r}\{-r\nabla^2\sigma + \partial_r[r^{-2}\partial_r(r^3\sigma) - 2\sigma]\} +$$

$$+ \nabla_1\{r^{-3}\partial_r(r^3\sigma) - 2r^{-1}\sigma\}$$

$$= \vec{r}\{r^{-1}\nabla^2\sigma\} + \nabla_1\{r^{-1}\sigma + \partial_r\sigma\}$$

$$= \vec{r}\left\{\frac{-l(l+1)}{r}\sigma\right\} + \nabla_1\{r^{-1}\partial_r(r\sigma)\}.$$

Collecting these we have

$$\mathbf{u} = \vec{r}\left\{\partial_r\psi - \frac{l(l+1)}{r}\sigma\right\} + \nabla_1\{r^{-1}\psi + r^{-1}\partial_r(r\sigma)\} - r \times \nabla_1\chi.$$

Therefore

$$U_l^m = \partial_r\psi_l^m - \frac{l(l+1)}{r}\sigma_l^m, \tag{A9a}$$

$$V_l^m = r^{-1}[\psi_l^m + \partial_r(r\sigma_l^m)], \tag{A9b}$$

and

$$W_l^m = \chi_l^m. \tag{A9c}$$

APPENDIX B. THE TRACTION ON A SPHERICAL SURFACE

Let $\underline{T}$ be the elastic stress tensor resulting from a displacement field $\mathbf{u}$. $\underline{T}$ is given by

$$\underline{T} = \lambda(\nabla \cdot \mathbf{u})\underline{I} + \mu(\nabla\mathbf{u} + \mathbf{u}\nabla) \tag{B1}$$

where $\mathbf{u}\nabla$ is simply the transpose of $\nabla\mathbf{u}$. The force (not stress) acting across a surface whose unit normal is $\vec{n}$ is given by $\vec{n} \cdot \underline{T}$, which is a vector quantity. We represent the force acting across a surface whose normal is the radius vector $\vec{r}$ by

$$\vec{r} \cdot \underline{T} = \vec{r}P + \nabla_1 Q - \vec{r} \times \nabla_1 R. \tag{B2}$$

Our problem is to relate the scalars P, Q and R to the scalars U, V and W which characterize the displacement field.

We note first that

$$\vec{r} \cdot \underline{T} = \lambda(\nabla \cdot \mathbf{u})\vec{r} + \mu\vec{r} \cdot \{\nabla\mathbf{u} + \mathbf{u}\nabla\}. \tag{B3}$$

The divergence of $\mathbf{u}$ can be expanded as

$$\nabla \cdot \mathbf{u} = (\vec{r}\partial_r + r^{-1}\nabla_1) \cdot (\vec{r}U + \nabla_1 V) \tag{B4}$$

since

$$\begin{aligned} \nabla \cdot (-\vec{r} \times \nabla_1 W) &= -\vec{r} \cdot (\nabla \times \nabla_1 W) \\ &= -\vec{r} \cdot (\vec{r} \times \nabla\partial_r W) \\ &= 0 \end{aligned}$$

because $\vec{r} \times \nabla\partial_r W$ must be normal to $\vec{r}$. Equation B4 can be written as

$$\nabla \cdot \mathbf{u} = \partial_r U + r^{-1}\nabla_1^2 V + \vec{r}\partial_r \cdot \nabla_1 V + r^{-1}\nabla_1 \cdot \vec{r}U. \tag{B5}$$

The third term vanishes since ∂_r commutes with ∇_1, and $\nabla_1\partial_r v$ is normal to $\vec{r}$. The fourth term is equal to $(2/r)U$ as may be seen by replacing $r^{-1}\nabla_1$ with $\nabla - \vec{r}\partial_r$, an equivalent expression. We then have

$$\nabla \cdot \mathbf{u} = \left(\partial_r + \frac{2}{r}\right)U + r^{-1}\nabla_1^2 v. \tag{B6}$$

The term $\vec{r} \cdot \{\nabla \mathbf{u} + \mathbf{u}\nabla\}$ in eq B3 is more difficult to deal with. In terms of the coordinate representation of u, (i.e. u_r, u_θ, and u_ϕ),

$$\vec{r} \cdot \{\nabla \mathbf{u} + \mathbf{u}\nabla\} = \vec{r}(2\partial_r u_r) + \vec{\theta}\left[\frac{1}{r}\partial_\theta u_r + r\partial_r\left(\frac{u_\theta}{r}\right)\right] + \\ + \vec{\phi}\left[\frac{1}{r\sin\theta}\partial_\phi u_r + r\partial_r\left(\frac{u_\phi}{r}\right)\right]. \tag{B7}$$

By inspection of eq 5 which explicitly gives the coordinate components of ∇_1, we see that eq B7 may be rewritten as

$$\vec{r} \cdot \{\nabla \mathbf{u} + \mathbf{u}\nabla\} = \vec{r}(2\partial_r u_r) + \nabla_1\left(\frac{u_r}{r}\right) + \\ + r\partial_r\left[\frac{1}{r}\left(\vec{\theta}u_\theta + \vec{\phi}u_\phi\right)\right].$$

We note that ∂_r commutes with $\vec{\theta}$ and $\vec{\phi}$. The expression in square brackets represents the non-radial portion of u and must therefore be identical with $\nabla_1 v - \vec{r} \times \nabla_1 w$. Since u_r is identical with U, we have

$$\vec{r} \cdot \{\nabla \mathbf{u} + \mathbf{u}\nabla\} = \vec{r}(2\partial_r v) + \frac{1}{r}\nabla_1 u + r\partial_r\left\{\frac{1}{r}\nabla_1 v - \frac{1}{r}\vec{r} \times \nabla_1 w\right\}$$

or

$$\vec{r} \cdot \{\nabla \mathbf{u} + \mathbf{u}\nabla\} = \vec{r}(2\partial_r u) + \nabla_1\left[\frac{u}{r} + r\partial_r\left(\frac{1}{r}v\right)\right] - \vec{r} \times \nabla_1\left[r\partial_r\left(\frac{1}{r}w\right)\right].$$

Combining the above results, we have

$$P = (\lambda + 2\mu)\partial_r u + \frac{2\lambda}{r}u + \frac{\lambda}{r}\nabla_1^2 v, \tag{B8a}$$

$$Q = \mu\left\{\frac{u}{r} + r\partial_r\left(\frac{v}{r}\right)\right\}, \tag{B8b}$$

and

$$R = \mu\left\{r\partial_r\left(\frac{w}{r}\right)\right\}. \tag{B8c}$$

APPENDIX C. NUMERICAL TECHNIQUES

We outline, briefly, in this appendix the numerical techniques used in this study to a) generate the suite of normal modes for a layered elastic sphere and b) evaluate various integrals of interest associated with these modes.

For a given l and ω, the generation of solution functions proceeds exactly as outlined in Section B. The matrix inversion required by eq 45 and 46 was not done explicitly. We chose instead to solve two sets of simultaneous linear equations. The Crout Reduction (Hildebrand, 1956) was found to be particularly convenient.

Bessel functions were generated by using Miller's well-known recurrence algorithm (Abramowitz and Stegun, 1968). One consequence of this technique is that the accurate evaluation of a spherical Bessel function for many values of its argument, as required, say, for integration, is a time-consuming process. For such applications it would perhaps be more efficient to numerically solve Bessel's equation, but computer memory limitations did not permit the additional coding this required.

In practice, the program was assigned a model and a value of l and proceeded to compute trail solutions for evenly spaced values of frequency. As the computation proceeded, indicator variables, as explained in Section B, were monitored for a change of sign, which was taken to indicate a zero crossing. When this occurred, an estimate was made of the location of the zero crossing and the algorithm described below was invoked to iteratively improve the estimate. In general, two applications of the following procedure sufficed to locate the eigenfrequency to within one part in 10^6.

Gilbert and Backus (1967) observed that Rayleigh's principle could be utilized to improve estimates of eigenfrequencies obtained by coarser methods. Suppose that for some frequency ω, near an eigenvalue, ω^*, we have computed a trial solution and find that the stress-free surface condition cannot be met. We may apply Rayleigh's principle, or perturbation theory, to the solution we have generated to estimate the change in ω the elimination of surface stress would produce. The first order estimate for this change is given by

$$\delta\omega = (8\pi\omega)^{-1} \frac{\{U_1(r_N)P_1(r_N) + l(l+1)V_1(r_N)Q_1(r_N)\}}{\int_0^{r_N} \rho r^2 \{U_1^2(r) + l(l+1)V_1^2(r)\}dr} . \tag{C1}$$

We will not derive eq C1 here. We then replace ω by $\omega + \delta\omega$ and repeat the process. We chose to terminate the iteration when $|\delta\omega/(\delta\omega + \omega)|$ fell below 10^{-6}.

The last point we wish to mention is the evaluation of integrals of the form

$$I = \int_0^u Z(u)du \tag{C2}$$

where Z is some operator on the solution functions, $U(r)$, etc. In general, we may expect Z to vary appreciably over a length L of about

$$L = \frac{2\pi V_p}{\omega} \tag{C3}$$

where V_p is the local compressional velocity. L is simply the wavelength of a compressional wave of angular frequency ω. In computing I, the program was designed to utilize steps not exceeding ϵL_i; where ϵ is a small ($\sim 3 \times 10^{-2}$) number and L_i is the scale length appropriate to a given shell. This technique yielded a reliably constant accuracy over many wide variations of scale without extracting undue computing labor for small values of ω.